



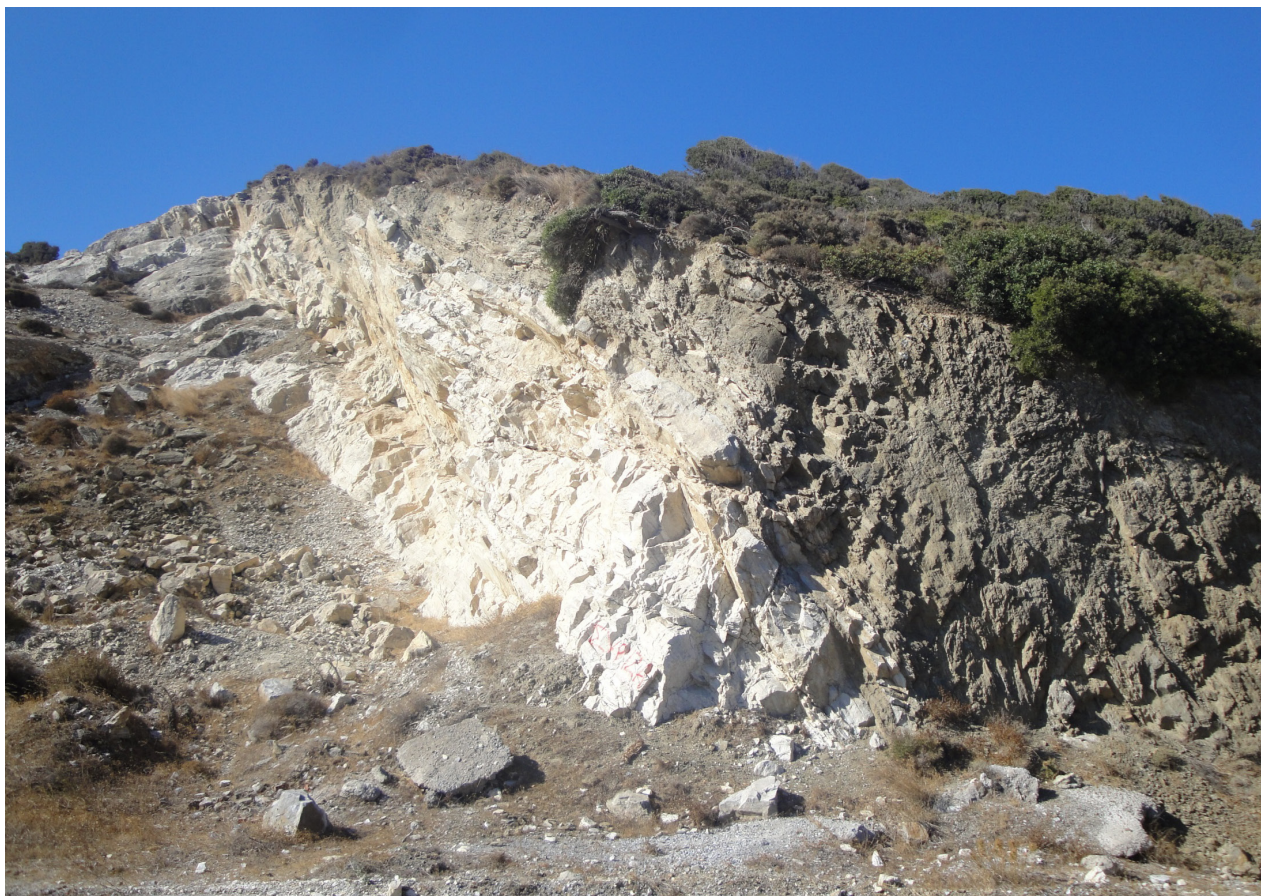
Stockholm
University

Master Thesis

Degree Project in
Geology 60 hp

One-dimensional modelling of stable isotopic and chemical profiles across a marble layer on Naxos, Greece

Madeleine Bohlin



Stockholm 2013

Department of Geological Sciences
Stockholm University
SE-106 91 Stockholm

One-dimensional modelling of stable isotopic and chemical profiles across a marble layer on Naxos, Greece

Adding constraints to the fluid infiltration event associated with the Miocene M2 metamorphism

Madeleine Bohlin

Abstract

A 17 meter thick marble band on the Greek island of Naxos show distinct alterations in isotopic and chemical compositions close to lithological contacts to adjacent schists. The alterations are a product of fluid infiltration during the M2 metamorphic event in the Miocene with peak metamorphic conditions of ca. 600°C and 6 kbar. Oxygen isotopic and chemical data across the profile have been fitted to two separate one-dimensional transport models. The models consider (1) coupled advective-diffusive transport (the pinned boundary model) and (2) advective transport through parallel and evenly spaced micro-cracks with transverse diffusion through the solid crystal network (the linear kinetic model). Best-fit estimates of fluid flow parameters are used to constrain the fluid flow regime. The results from this study suggest that the metamorphic fluid was channelled along grain boundaries and that geochemical tracers were transported advectively with a transverse diffusive component into the wall rock limiting the rate of front propagation. The calculated exchange rate of the diffusive component is $9.46 \times 10^{-13} \text{ s}^{-1}$. This means that previous conclusions drawn about transport mechanisms and equilibrium conditions during the prograde fluid infiltration event on Naxos needs to be revised. The total volume of fluid infiltrating the rock (time-integrated fluid flux) is calculated to $1.05 \pm 0.02 \text{ m}^3/\text{m}^2$. The duration of the infiltration event is calculated as $113\,000 \pm 20\,000$ years, giving a time-averaged fluid flux rate of $2.98 \times 10^{-13} \pm 5.28 \times 10^{-14} \text{ m}^3/\text{m}^2/\text{s}$.

Contents

Introduction	4
Previous workers	5
Geological background	7
Geology of Locality B	8
Theoretical background	9
Tracer transport theory.....	9
The pinned boundary model: advective-diffusive transport with fluid-solid equilibrium.....	11
Linear kinetic exchange model: tracer transport with kinetic control on fluid-solid exchange.....	15
Concentration ratio profiles	20
Methods	21
Field work	21
XRF measurements	22
Stable isotopic analysis	23
Results	24
Rock chemistry.....	24
Isotopic profiles.....	26
Discussion	29
Best-fit parameterization	29
Fitting data to the pinned boundary model.....	29
Fitting data to the linear kinetics exchange model	29
Results from model fitting.....	30
Oxygen isotopic profile	31
Carbon isotopic profile	33
Element profiles	33
Volumetric solid-fluid partition coefficient.....	35
Duration of fluid infiltration.....	35
Fluid flux calculations	37
Composition of the infiltrating fluid.....	37
Calculations of element concentrations of the fluid	38

Effects of retrograde fluid infiltration at Locality B.....	39
Conclusions.....	43
Acknowledgements	44
References	45
Appendix A – Derivation of transport equations	49
Appendix B – Results from XRF analysis	53

Introduction

Pelites and carbonate rocks are the major sources of chemically bound fluid components in the Earth's crust. Pelitic rocks contain approximately 5wt% chemically bound H₂O which adds up to a total of $1.1-1.3 \times 10^{20}$ kg of H₂O in the crust (Garrels and MacKenzie, 1987; Walther and Orville, 1982). Carbonate rocks contain 44-48wt% chemically bound CO₂ meaning that the carbonate reservoir in the Earth's crust contains $0.7-2.3 \times 10^{20}$ kg of CO₂ (Garrels and MacKenzie, 1971). These numbers are equivalent to the mass of water in one tenth of the Earth's oceans, and five orders of magnitude greater mass of CO₂ than there currently is in our atmosphere.

The fluid components are released from the mineral structures in devolatilisation reactions during prograde metamorphism mainly at greenschist, blueschist and amphibolite facies conditions. The released fluids are buoyant and migrate upwards through the crust and are mainly channelled through permeable lithologies and structurally controlled pathways (e.g. Skelton et al., 1995;2000). The metamorphic fluids interact with the rock and give rise to chemical alteration and transport of heat and matter between the Earth's mantle and crust. The potential impact on the Earth's hydrological and carbon cycles are hard to determine since fluid flux rates are hard to constrain. The magnitude and flux of metamorphic fluids cannot be measured directly but needs to be evaluated from indirect geochemical and petrological evidence resulting from infiltration driven alterations. The effects of fluid infiltration are especially large where two lithologies meet. Individual fluid and rock reservoirs have characteristic chemical and isotopic signatures so infiltration of a fluid derived from, or in equilibrium with a chemically different rock creates boundary layers of alteration close to the lithological contacts. The displacement of an initially sharp geochemical front between the lithologies provides a lasting record of fluid flow and is directly related to the total volume of fluid that has infiltrated the rock (the time-integrated fluid flux) as well as the mechanisms of fluid transport.

The shape of the geochemical or isotopic profile created by fluid infiltration can be modelled against well-known one-dimensional transport equations describing fluid flow through a porous medium. The models consider that alteration results from a combination of advection by the fluid phase, and diffusive or kinetically limited exchange between the fluid and the rock. Best-fit estimates of dimensionless fluid flow parameters from these transport equations allow interpretation of the fluid flow regime and the nature of the metamorphic environment.

The Greek island of Naxos forms the centre of a metamorphic core complex with several recorded fluid infiltration events (Rye et al., 1976; Baker et al., 1989; Bickle and Baker, 1990). The geology mainly consists of marble layers which are imbedded in thick sequences of metapelitic rocks with increasing metamorphic grade towards the centre of the island. The marbles are particularly informative, since they represent distinct compositional anomalies within the pelitic sequence. These conditions make Naxos an optimal place to study the effects of metamorphic fluid flow.

Previous workers

The rocks on Naxos have been studied by many, and previous work on isotopic compositions and fluid fluxes provide a firm base for this study. Rye et al., (1976) documented a progressive decrease in $\delta^{18}\text{O}$ in silicates with increasing metamorphic grade. They suggested that the rocks had been in equilibrium with a metamorphic fluid that ranged in oxygen isotopic composition, starting at 15‰ in the lower grade schists, to 8.5‰ in the high grade migmatite centre. They also discovered that marble bands which are imbedded in the schists have narrow boundary layers close to lithological contacts, which show signs of isotopic alteration. These boundary layers increase in width with increasing metamorphic grade, and also show an asymmetry with broader layers at stratigraphically lower lithological contacts. Rye et al., (1976) propose that these isotopic boundary layers were caused by infiltration of a metamorphic fluid which was flowing in an upward direction. Schuiling and Kreulen (1979) proposed that the fluid was mantle derived CO_2 which systematically shifted $\delta^{13}\text{C}$ values in fluid inclusions and calcites within the schists to values lower than original marine values observed in the interior of the marble bands. This statement was supported by later work by Kreulen (1980; 1988) on fluid inclusions that revealed a fluid composition with 60-90vol% CO_2 . These results together with his argument that the influx of the hot CO_2 was responsible for the metamorphic event on Naxos are quite controversial and argued against by several authors (Bickle and McKenzie, 1987; Jansen et al., 1989; Baker et al., 1989). Observations that contradict such a high CO_2 content in the metamorphic fluids include mineral findings (epidote, clinozoisite and zoisite are found throughout the metamorphic sequence on Naxos, which require a fluid with X_{CO_2} less than 0.2 (Jansen et al., 1989)) and peak metamorphic relationships between $\delta^{18}\text{O}$ and $\delta^{13}\text{C}$ (Baker et al., 1989).

Baker et al., (1989) further document at least two separate events of fluid infiltration of water-rich fluids with X_{CO_2} of no more than 0.3. The first infiltrating fluid was derived from dehydration of underlying schist and is responsible for the alteration boundaries at lithological

contacts. This prograde fluid had a $\delta^{18}\text{O}$ value of ca. 12 to 16‰ and $\delta^{13}\text{C}$ of -3 to -12‰. The second fluid flow event observed by Baker et al., (1989) was responsible for the formation of retrograde calc-silicate veins. The retrograde fluid was likely derived from the movement of melts produced during peak metamorphism and post-peak recrystallization of the migmatite associated with the M2 metamorphic event. This second fluid is reported as having $\delta^{18}\text{O}$ of less than 10‰ and $\delta^{13}\text{C}$ ranging from -5 to -7‰.

The shape of oxygen isotopic profiles across several marbles of varying metamorphic grade was modelled to a coupled advective-diffusive transport model by Bickle and Baker (1990). They calculate time-integrated fluid fluxes ranging 0.2-1 m^3/m^2 for the Naxos marbles and concluded that the goodness-of-fit between the model and their data validates the assumption which the model is based upon, including (i) constant porosity throughout the marble and (ii) local fluid-solid equilibrium. These assumptions are however questioned by Lewis et al., (1998) after micro-scale isotopic measurements. They find that individual calcite grains in marbles contain isotopic profiles with $\delta^{18}\text{O}$ values of 25‰ in grain centres and values reaching as low as 2‰ at grain boundaries. These results suggest that the fluid may have been derived from surface waters (meteoric or seawater) and implies that the assumption of local fluid-solid equilibrium cannot be applied on the Naxos marbles.

Aim of study

The aim of this study is to fit isotopic and chemical data to two one-dimensional transport equations describing (1) coupled advective-diffusive transport and (2) advective transport through parallel and evenly spaced micro-cracks with transverse diffusion through the solid crystal network perpendicular to the cracks. The first model (the *pinned boundary model*) was first applied on the Naxos marbles by Bickle and Baker in 1990, but will be revised with additional isotopic and chemical data. The second model (the *linear kinetic exchange model*) will be introduced to this locality for the first time. Best-fit estimates of the parameters governing these equations will be used to calculate a time-integrated fluid flux, the duration of fluid infiltration and with that the time-averaged fluid flux. The best-fit results will also be used to put constraints on the chemistry of the infiltrating fluid and its potential origin as well as the transport mechanism responsible for tracer transport in the Naxos marbles at metamorphic conditions.

Geological background

Naxos is situated in the southern Aegean Sea and is the largest island in the Attic-Cycladic Massif. The Attic-Cycladic Massif forms a belt of metamorphic rocks stretching from the Greek mainland in the west to Turkey in the east. The geodynamic evolution of this area is associated with the Cenozoic

convergence between Africa and Eurasia, and subduction of the Aegean slab (Seward et al., 2009; figure 1). Naxos is situated in the back-arc basin to the north of the subduction zone and the geodynamic evolution of the last 40 Ma has been controlled by slab rollback (Fyktilas et al., 1984).

The rocks in the Attic-Cycladic Massif show signs of blueschist, greenschist and amphibolite facies metamorphism (Jansen and Schuiling, 1976; Buick and Holland, 1989) as well as signs of decompression and cooling caused by exhumation during an extensional phase in the Miocene (Lister et al., 1984). The high-pressure low-temperature

blueschist facies metamorphic event (named M1) occurred in the Eocene approximately 45 ± 5 Ma (Wijbrans and McDougall, 1988). Except for in the south-east of Naxos where there are some blueschist rocks preserved (Avigad and Garfunkel, 1991) the M1 event is overprinted by a Barrovian type metamorphic event (named M2). The M2 event occurred in the Miocene and reached peak metamorphic conditions of $670\text{--}700^\circ\text{C}$ and 6 ± 2 kbar (Jansen and Schuiling, 1976; Buick and Holland, 1989) approximately 20-15 Ma (Wijbrans and McDougall, 1988). As a consequence of late folding, the overprint has been exposed as an elliptical structural dome with the long axis trending NNE-SSW, the same as the mineral lineation of the metamorphic rocks (Baker and Matthews, 1994). There are a series of isograds lying sub parallel to the stratigraphic layering, with temperatures increasing from

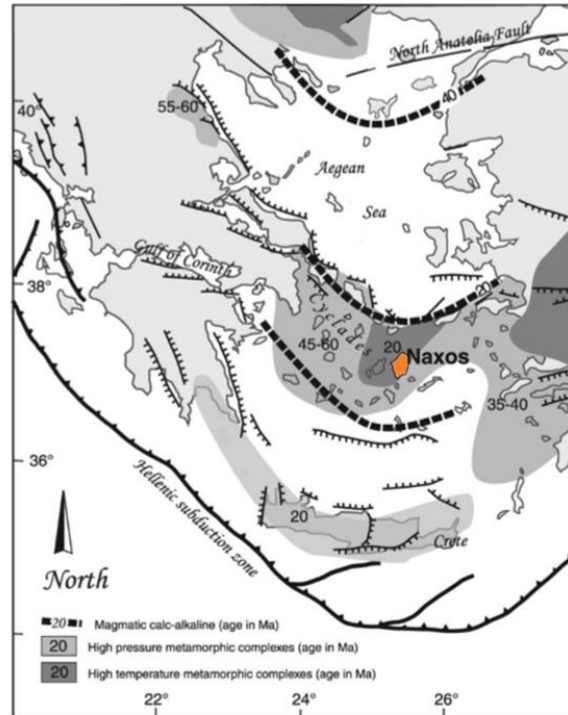


Figure 1 – Regional tectonic setting of the Aegean Sea showing the position of Naxos in relation of the Hellenic subduction zone (modified from Seward et al., 2009).

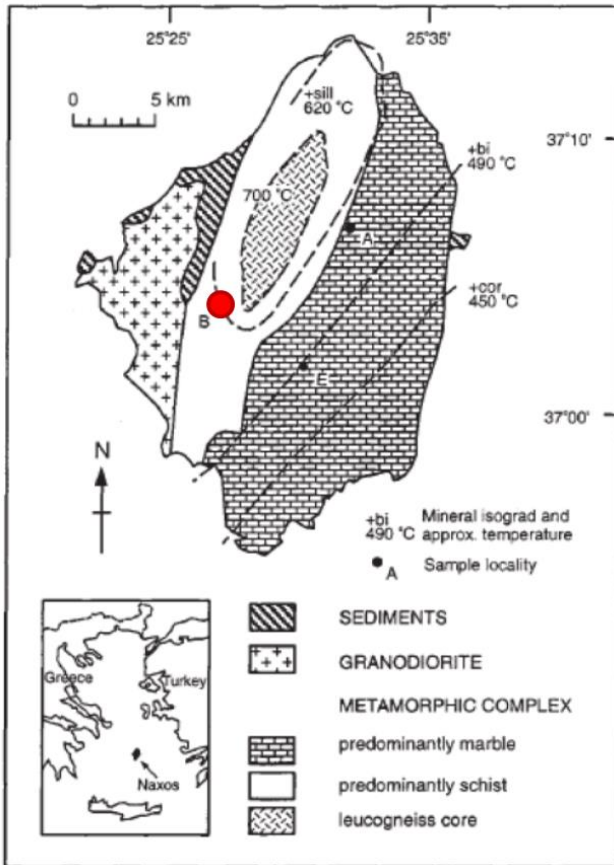


Figure 2 - Schematic image of Naxos including main lithological units and isograds resulting from the Miocene prograde metamorphic event (modified from Lewis et al., 1998).

approximately 450°C in the stratigraphically higher, lower grade units to 700°C in the core of the complex which has undergone partial melting (Baker et al., 1989).

The geology on Naxos (figure 2) consists of the leucogneiss migmatitic core, located at the centre of the crystalline complex. The core is overlain by a 7 km thick sequence of meta-sedimentary rocks dominated by siliciclastic schists and gneisses in its lower part and by marbles in its upper part (“lower” and “upper” series respectively after Jansen and Shuiling, 1976). The west of Naxos

consists of post-metamorphic granodiorite intrusions dated to 13.6-12.1 Ma (Wijbrans and McDougall, 1988) and unmetamorphosed Tertiary sediments emplaced during extensional deformation (Lister et al. 1984).

Geology of Locality B

The area of interest in this paper is Locality B (using the same notation as Baker et al., 1989) which is an old quarry laying to the east of the migmatitic core, in the schist-dominated part of the island (figure 2). The outcrop consists of an approximately 17 meter thick marble band oriented at 280° and dipping 50°, imbedded in a series of kyanite-staurolite zone pelites (figure 3). Estimated peak M2 metamorphic conditions are 600±50°C (Baker et al., 1989).

The lithology varies within the marble with the first 30 cm consisting of a coarse white calcite marble. After that the marble is brown in its appearance with narrow streaks of layer parallel brown and dark minerals of hematite and margarite (Baker et al., 1989). Three meters into the

profile the lithology consists of alternating light grey and darker marble with small amounts of graphite and tremolite (Baker et al., 1989). Towards the upper contact the marble becomes progressively darker and at 16 meters the marble is dominantly dark grey. About half a meter before the upper lithological contact there is an intercalated band of schist approximately 30 cm wide. Right before the upper contact the lithology consists of a narrow band of coarse and white marble.



Figure 3 – Photo of Locality B on Naxos. The 17 meter wide marble band is imbedded in thick sequences of kyanite-staurolite zone schists.

Theoretical background

Tracer transport theory

Geochemical tracers can be transported by several means, including advection, diffusion and dispersion. In the metamorphic setting, matter is mainly transported by advection, meaning it is transported by the bulk motion of the fluid phase through the solid network. This process creates a sharp geochemical front. What broadens the initially sharp front is diffusion and dispersion of the geochemical tracer. Diffusion can be described as the random movements of particles which arises due to chemical gradients, causing the particles to move in a way that the gradients even out. The diffusion through the solid network is several orders of magnitudes slower than through the fluid. Dispersion can be separated into hydrodynamic and

kinetic dispersion. Hydrodynamic dispersion causes geochemical tracers to spread out due to velocity differences within the fluid phase or between fluid conduits, while kinetic dispersion arises from differences in rate of exchange between the fluid and solid, and is strongly influenced by the mechanism of fluid transport (Bickle, 1992).

Chromatographic modelling can be used to describe the coupled advective displacement and diffusive and dispersive broadening of an initial step in geochemical or isotopic composition. The shape of an advectively displaced geochemical profile depends on the time-integrated fluid flux (the total volume of fluid that has passed through a unit area of rock), the relative concentration of the tracer between the fluid and solid phases, kinetic dispersion or diffusion in the fluid and solid phase and the nature of the exchange process between the fluid and solid. The displacement of the chemical profile across the boundary layer at a lithological contact can therefore be used to put constraints on a number of aspects of the fluid flow regime (e.g. Rye et al., 1976; Bickle and McKenzie, 1987; Baumgartner and Rumble, 1988, Bickle and Baker, 1990; Bickle, 1992).

Table 1 – List of symbols, constants and units

Variables	Definition	Value	Units
B	Crack half-spacing (grain half-diameter)	0.005	m
$C_s, C_f, C_{s\infty}$	Concentration (by mass) of geochemical tracer, (s) in solid phase (f) in fluid phase, (s, ∞) when rock is in equilibrium with fluid		ppm, ‰
D_s, D_f	Diffusion coefficient in (s) solid phase and (f) fluid phase	$D_s: 3.15 \times 10^{-19}$	m^2/s
D_{eff}	Effective diffusivity of the two phase medium = $\phi D_f \tau$		m^2/s
h	Length scale, for advective-diffusive transport h is the thickness of marble layer, for advective-kinetic exchange $h = \omega t$		m
I_0	Modified Bessel function order 0		
K_d	Solid/fluid partition coefficient by mass		
K_v	Solid/fluid partition coefficient by volume		
N_d	Damköhler number		
N_{Pe}	Peclet number		
t	Time		s
z	Distance in direction of fluid flow		m
Z_{GF}	Distance to geochemical front		m
α	Isotopic fractionation factor		
ϕ	Porosity of the rock		
κ	Exchange rate constant for linear kinetic exchange		
ρ_f, ρ_s	Density of the (f) fluid and (s) solid	f: 1000 s: 2700	kg/m^3 kg/m^3
τ	Tortuosity of the fluid flow path		
ω	Flow velocity of the fluid		m/s

The pinned boundary model: advective-diffusive transport with fluid-solid equilibrium

The differential equation describing coupled advective-diffusive transport of a geochemical tracer moving perpendicular to the lithological contact is derived from the continuity equation describing the conservation of mass (Appendix A). The porosity is assumed to be constant throughout the marble layer, and the rate of advection is assumed to be slow relative to the rate of exchange between the rock and fluid. The model therefore assumes local grain-scale equilibrium. If equilibrium is maintained at any given time, the effect of reaction or exchange rates (kinetic dispersion) on the shape of the profile can be ignored, and the broadening of the isotopic or geochemical front will be caused only by coupled advection and diffusion. This type of equation has been used extensively (Hofmann, 1972; Bickle and McKenzie, 1987; Baumgartner and Rumble, 1988) and is given by Bickle (1992) as

$$\left(\varphi + \frac{\rho_s K_d}{\rho_f} (1 - \varphi) \right) \frac{\partial C_f}{\partial t} + \omega \varphi \frac{\partial C_f}{\partial z} = \varphi D_{eff} \frac{\partial^2 C_f}{\partial z^2} \quad (1)$$

where t is time, z the direction of fluid transport, C_f the concentration of the geochemical tracer in the fluid phase flowing with a velocity ω , through a porosity φ . ρ_s and ρ_f are the densities of the solid and fluid phases respectively, K_d is the distribution or partition coefficient by mass of the tracer between the solid and fluid phase and D_{eff} is the effective diffusion coefficient of the two phase material, which can be approximated by

$$D_{eff} = \varphi D_f \tau \quad (2)$$

where D_f is the diffusivity in the fluid phase and τ the tortuosity.

It is convenient to transform equation (1) to non-dimensional variables z' , C' and t' , where:

$$z = h z' \quad (3)$$

$$t = \frac{h^2}{D_{eff}} \left(\frac{\rho_s K_d}{\rho_f} (1 - \varphi) + \varphi \right) t' \quad (4)$$

$$C - C_1 = (C_2 - C_1)C' \quad (5)$$

where h is an appropriate length scale, here chosen as the width of the marble layer (16.9 m). C_1 is the initial fluid composition in the schist, and C_2 is the initial fluid composition in the marble. The transformations re-scales the variables so that C' and z' ranges from 0 to 1.

Having the variables dimensionless allows the use of any appropriate length or time scales, and the minimum number of dimensionless constants that control the fluid flow can be obtained. The transformations reduce equation (1) to:

$$\frac{\partial C'}{\partial t'} + N_{Pe} \frac{\partial C'}{\partial z'} = \frac{\partial^2 C'}{\partial z'^2} \quad (6)$$

where N_{Pe} is the dimensionless Peclet number which describes the coupled advection and diffusion in the Z-direction. N_{Pe} is given by:

$$N_{Pe} = \frac{\omega \phi h}{D_{eff}} \quad (7)$$

The Peclet number is a measure of the importance of advective transport relative to diffusive transport. The value of N_{Pe} is large when advection dominates and the geochemical front is sharp, and small when diffusion and broadening of the geochemical front becomes more pronounced.

The solution for equation (6) depends on the chosen initial and boundary conditions. The initial isotopic distribution across the profile is approximated as a step function (figure 4A), with the concentration within the marble layer (where z ranges from 0 to 16.9 meters) being constant at C_2 . Re-scaling using equations (3) and (5) gives us an initial condition such that, when $t=0$:

$$C' = 1 \quad \text{at} \quad 0 < z' < 1 \quad (8)$$

The porosity is assumed constant within the marble, but far less than the porosity of the adjacent schist. This porosity difference causes the fluid to be channelled in the schist, leaving only a smaller portion infiltrating the less permeable marble (compare figures 4B and 4D and

the “*Uniform flow model*” of Bickle and Baker, 1990). The fluids are transported relatively fast within the schist, and the volume of fluid is assumed to be infinitely large compared to that infiltrating the marble. This causes the concentration of chemical or isotopic tracers at the lithological contact to be buffered to that of the fluid in the schist (figure 4D).

The boundary conditions are set so that the concentrations at the lithological contacts ($z=0\text{m}$ and $z=16.9\text{m}$) are constant, or *pinned*, to the constant C_1 , for all times. Using equations (3) and (5) again expresses the boundary conditions, for all times, as:

$$C' = 0 \quad \text{at} \quad z' = 0 \quad \text{and} \quad z' = 1 \quad (9)$$

The initial and boundary conditions given by expression (8) and (9) give us the final analytical solution to equation (6) (from Bickle and McKenzie, 1987):

$$C' = 2\pi e^{(N_{Pe} z'/2)} \sum_{n=1}^{\infty} \frac{n}{(N_{Pe}/2)^2 n^2 \pi^2} [(-1)^n e^{(N_{Pe}/2)} - 1] e^{-t'((N_{Pe}/2)^2 + n^2 + \pi^2)} \sin(n\pi z') \quad (10)$$

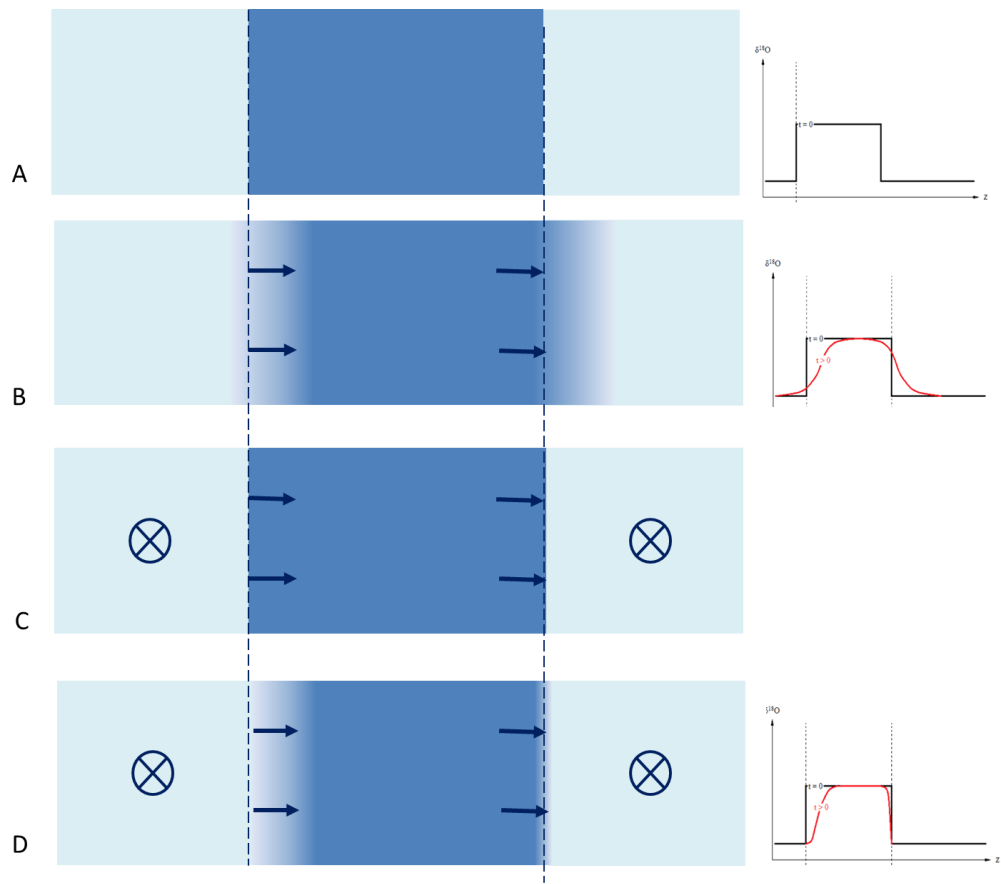


Figure 4 – Schematic image illustrating the pinned boundary transport model. The light blue areas represent the fluid that is in chemical and isotopic equilibrium with the schist (isotopically light) and the dark blue area represents the fluid that is in equilibrium with the marble (isotopically heavy). The red graphs illustrate the shape of the front modified by fluid flow compared to an initial geochemical step (black line). Figure **(A)** illustrates the initial condition, at $t=0$, where the chemical or isotopic front is sharp and has a step function across the different lithologies. Figure **(B)** illustrates what would happen if the porosity of the schist and marble was equal. The fluid would be transported uniformly by advection in one direction across the lithological boundaries and the front would be broadened by diffusion. Note that the effects of diffusion would also be visible behind the geochemical front, in the schist. Figure **(C)** illustrates a more realistic scenario where the marble is relatively impermeable compared to the schist. This causes the fluid to be channelled within the schist and the dominant fluid flow direction will be parallel to the lithological contact (into the paper in figures C and D, as illustrated by the crossed circles). Only a small portion of the fluid will start to infiltrate the less permeable marble perpendicular to the lithological contact **(D)**. The infiltrating fluid will be transported by advection and the propagating front will be broadened by diffusion. Note that the chosen boundary conditions remove all diffusion into the schist and the concentration on the lithological contacts will be pinned to the composition of the fluid in the schist. The relationship between the magnitudes of advection and diffusion is describes by the Peclet number, and can also be read from the morphology of the front, with a sharp front corresponds to a high Peclet number, and a broad front corresponding to a low Peclet number.

Linear kinetic exchange model: tracer transport with kinetic control on fluid-solid exchange

The pinned boundary model assumes local grain scale equilibrium between the fluid and the solid, and a constant porosity allowing pervasive fluid flow. However, if the rate of advection is greater than the rate of exchange between the fluid and the solid (i.e. the fluid moves so fast that the exchange between the fluid and solid does not have time to go to completion), the assumption of equilibrium is not valid. Lewis et al., (1998) showed that the marbles on Naxos in fact appear to be out of equilibrium on the grain scale level, by showing oxygen isotopic gradients within individual calcite grains. At such conditions the broadening of the geochemical front is caused by kinetic dispersion in addition to diffusion and the propagation of the fluid front is determined by (1) the relationship between the rate of advection and rate of exchange between the fluid and solid and (2) the kinetic law governing the exchange between the fluid and solid and (3) the geometry of the porosity. The relationship between the advection and exchange rates is given by the Damköhler number (N_D) which decreases as dispersion increases and the front broadens, and the kinetic law governing the exchange depends on the slowest mechanism in the exchange process, which may be diffusion-controlled and include transport of the tracer away from the fluid conduits by diffusion through either the fluid or solid phases.

The geometry of the porosity controls the transport mechanism. Pervasive flow of the fluid demands an interconnected network of pores with a dihedral angle, θ (angle between solid grains) less than 60° . This is often assumed in metamorphic conditions where the rock is in textural and chemical equilibrium (e.g. Bickle and McKenzie, 1987). However, marbles seldom exhibit dihedral angles less than 60° at amphibolite facies conditions and are in fact quite impermeable in regards of porous fluid flow (Wark and Watson, 2003). Several studies suggest that metamorphic fluids are channeled through conduits and (micro) cracks rather than through a uniform porosity (Bickle, 1992; Lewis et al., 1998). This greatly changes the fluid flow regime and interaction with the rock. If the rock is assumed to consist of equally spaced cracks, and the fluid phase is moving relatively fast along the cracks (z-direction) the diffusion in the same direction can be ignored. The propagation of the geochemical or isotopic front will then be determined by the rate of exchange between the rock and the fluid.

Bickle (1992) showed that tracer transport through a fluid flow geometry consisting of equally spaced cracks, with transverse diffusion of the geochemical tracer into the wall rock (figure 6) can be approximated by a linear kinetic exchange law. The differential equations governing the concentration of tracer under such conditions are given by Lassey and Blattner (1988) as:

$$\frac{\partial}{\partial t}(\Phi' C_f + C_s) + \Phi' \omega \frac{\partial C_f}{\partial z} = 0 \quad (11)$$

$$\frac{\partial C_s}{\partial t} = \kappa(C_{s,\infty} - C_s) \quad (12)$$

where C_f and C_s are the concentrations of the geochemical tracer in the fluid and solid respectively, ∞ denotes the concentration of the rock at an infinite position where the fluid and rock are in equilibrium, ϕ is the porosity, κ is the exchange rate constant, ω is the velocity of the fluid and ϕ' is here given by:

$$\Phi' = \frac{\phi \rho_f}{\rho_s(1 - \phi)} \quad (13)$$

Equation (11) is derived from the continuity equation describing the conservation of mass (see Appendix A) and equation (12) specifies the fluid-solid exchange kinetics. As seen in equation (12) the magnitude of the rate of change will be high when the concentration is far from the equilibrium concentration. As time goes, C_s will asymptotically approach $C_{s,\infty}$ and the rate of change in the concentration with time will approach zero (i.e. equilibrium).

The initial concentration of the marble (for $z > 0$, $t = 0$) is assumed to be equal to the constant C_2 . As time passes ($t > 0$) the concentration at the lithological boundary ($z = 0$) is considered to be *pinned* in the same sense as in the pinned boundary model, to a constant C_1 .

To simplify the problem, the initial and boundary conditions and the variables in equation (11) and (12) are made non-dimensional by the transformations (modified from Lassey and Blattner, 1988):

$$t = \frac{ht'}{\omega} \quad (14)$$

$$z = hz' \quad (15)$$

$$C_s = C_{s2} - (C_{s2} - C_{s1})C'_s \quad (16)$$

$$C_f = C_{f2} - (C_{f2} - C_{f1})C'_f \quad (17)$$

where C_1 and C_2 are the constant bounding concentrations and h is an appropriate length scale. Using equations (14) - (17) expresses the initial and boundary conditions as such:

$$C'_s = 0 \text{ for } z' > 0 \quad \text{at } t' = 0 \quad (18)$$

$$C'_s = 1 \quad \text{at } z' = 0 \quad \text{for } t' > 0 \quad (19)$$

and transforms equations (11) and (12) to:

$$\frac{\partial}{\partial t'}(\Phi' C'_f + C'_s) + \Phi' \frac{\partial C'_f}{\partial z'} = 0 \quad (20)$$

$$\frac{\partial C'_s}{\partial t'} = N_D(C'_{s,\infty} - C'_s) \quad (21)$$

where N_D is the dimensionless Damköhler number which describes the ratio between the rate of exchange to the rate of advection:

$$N_D = \frac{\kappa h}{\omega} \quad (22)$$

A high Damköhler number means that the exchange rate is fast compared to the fluid velocity, which causes a decrease in kinetic dispersion and a sharper geochemical front (figure 5).

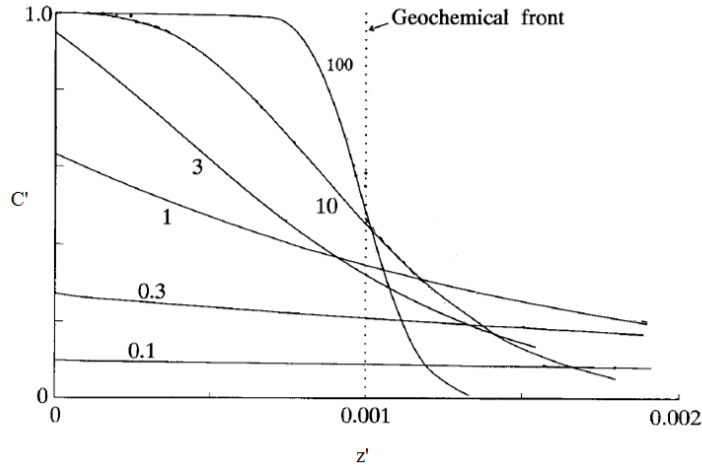


Figure 5 – Examples of different shapes of the geochemical front caused by advective transport with kinetic control on the fluid-solid exchange. The different lines corresponds to different values of the Damköhler number, N_D (the numbers in the figure). As the kinetic dispersion of the tracer increases, the geochemical front is broadened, or flattened out, and the Damköhler number decreases (Image modified from Bickle, 1992).

Given the chosen initial and boundary conditions, the solutions to equation (11) and (12) are given by Lassey and Blattner (1988) as:

$$C'_s = K \left\{ N_D (t' - z'), \quad \frac{N_D z'}{\Phi'} \right\} \quad (23)$$

$$C'_f = 1 - K \left\{ \frac{N_D z'}{\Phi'}, N_D (t' - z') \right\} \quad (24)$$

If the length scale h in equation (14) and (15) is chosen as the distance of the advectively displaced fluid front (ωt) and assuming that porosities are small, the expressions can be further simplified to (Skelton et al., 2005):

$$C'_s = K \left\{ N_D, \frac{N_D}{Z_{GF}} \right\} \quad (25)$$

$$C'_f = 1 - K \left\{ \frac{N_D}{Z_{GF}}, N_D \right\} \quad (26)$$

Where $K \{ X, Y \}$ is the K-function from Lassey, (1982):

$$K\{X, Y\} = \int_0^x e^{-u-y} I_0(2\sqrt{uy}) du \quad (27)$$

where I_0 is the modified Bessel function order zero.

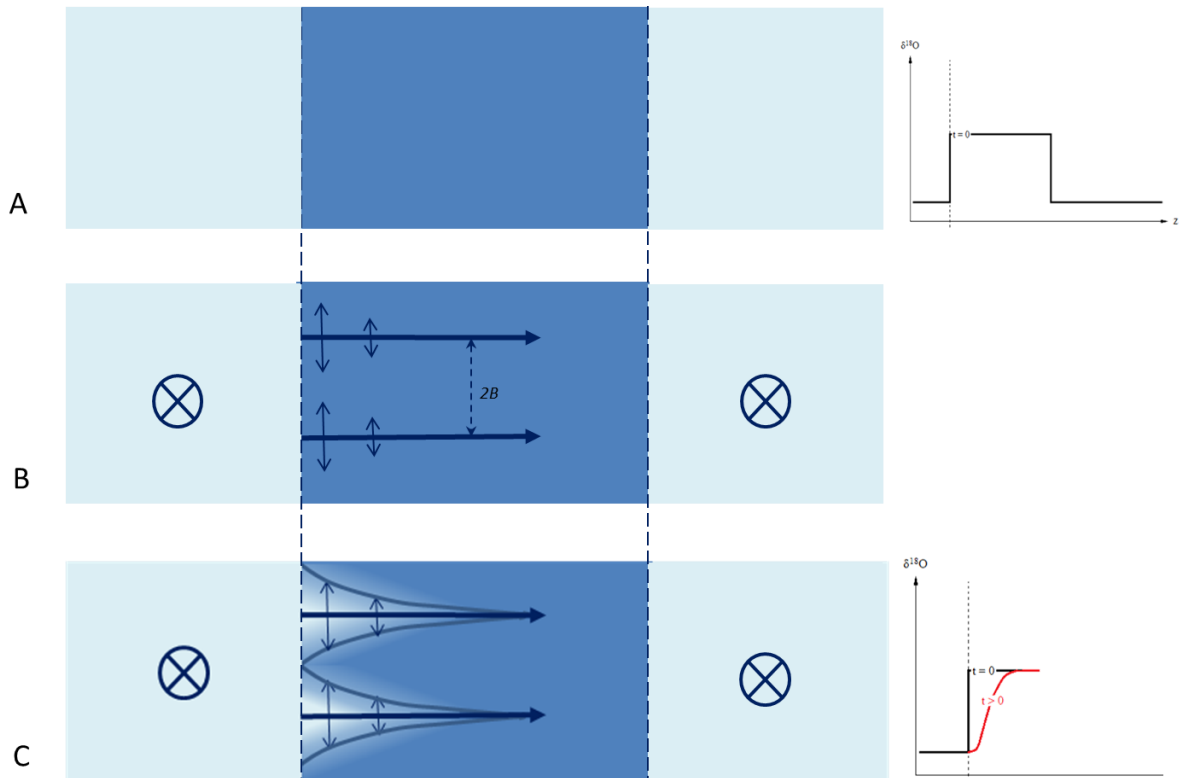


Figure 6 – Schematic image illustrating the linear kinetic exchange model as an approximation for crack flow with transverse diffusion into the wall rock. The light blue areas represent the fluid that is in chemical and isotopic equilibrium with the schist (isotopically light) and the dark blue area represents the fluid that is in equilibrium with the marble (isotopically heavy). Figure **(A)** illustrates the initial condition, at $t=0$, where the chemical or isotopic front is sharp and has a step function across the different lithologies. Figure **(B)** illustrates the considered flow geometry with evenly spaced parallel cracks allowing advective transport of the tracer components in the z -direction. The broadening of the front is caused by transverse diffusion into the wall rock through either the fluid filled porosity or through the solid crystal network. The spacing between the cracks has the distance $2B$. The boundary concentration is pinned (as in the pinned boundary model) to a constant C_1 and the dominant fluid flow is layer parallel within the schist. Figure **(C)** illustrated the effect of the transverse diffusion. Cross-sections of the flow will plot as the red line in the graph to the right.

Concentration ratio profiles

During regional metamorphism of carbonate rocks there is a significant mass transfer of non-volatile rock-forming elements (e.g. Ague, 2003). The loss or gain of elements varies locally and the mobility of these elements may illuminate processes of crustal fluid-rock interaction.

The concentration of an element is determined by its mass per kg of rock. Gains or losses of elements during fluid-rock interaction changes the overall rock volume and may dilute or concentrate specific elements even though their mass has stayed constant. In order to get around this problem it is common to normalise tracer concentrations to an immobile reference species such as Zr, Ti or a REE. The mass of a perfectly immobile element is constant and unaffected by the interaction between the fluid and rock, but its concentration will change due to overall mass and volume changes of the rock caused by addition or loss of other elements. If elemental concentrations across the marble profile are normalised against an immobile element it is possible to eliminate the effect of addition or removal of other elements.

An immobile reference species is identified by a sharp and great difference in concentration between the schist and marble, as well as a relatively uniform distribution within each lithology.

By normalising chemical profiles of the rock to an immobile reference frame it is possible to distinguish between mass addition and loss of elements from volume changes in the rock. Another effective way to quantitatively assess chemical changes is to normalise the element concentrations of the altered rock against protolith concentrations. The term protolith is used in a general way and denotes some previous stage in the rocks history.

The concentration of the altered stage relative the protolith is then compared to the a reference species ratio, R, defined as

$$R = \frac{C_i^*}{C_i^0} \quad (28)$$

where C_i^0 is the concentration of the immobile reference species in the protolith, and C_i^* is the concentration of the immobile reference species in the altered rock. If the protolith was completely homogeneous and the chemical analyses contain no errors, the ratio R of all *perfectly* immobile elements would be exactly the same throughout the profile. This is of course the ideal case which is not very realistic, and R varies somewhat along the profile.

A reference species R-value greater than 1 indicates an overall rock mass loss and volume decrease due to removal of mobile elements, and the residual elements in the rock have therefore been enriched, whereas an R-value less than 1 indicates an overall mass gain and increase in rock volume. Comparing the concentration ratios of other elements to the reference species ratio provides an effective mean of assessing which elements that have been added or removed from the rock. An element concentration ratio with a greater value than that of the reference species has been added to the rock, while one with a value less than the reference has been removed.

Methods

Field work

Both lithological contacts between the marble and adjacent schists at Locality B are exposed, although not along a continuous profile, so the sampling profile needed to be constructed in two separate segments across the marble band, with the first segment starting in the main quarry situated upslope approximately 20 meters from the road (figure 7). The first segment starts one meter into the schist from the lithological contact at -1 m (the contact is located at 0 m), and continues to 14.6 meters. The marble layer can then be followed down the slope to the second segment which lies by the road. The profile continues at 14.6 meters, passed the second contact at 16.9 meter and ends at 17.7 meters, in the schist.

The profile was constructed at a 20° angle from the normal of the stratigraphically lower lithological contact. This angle has been corrected for and the final profile is perpendicular to the layering of the marble.

The profile was sampled for isotopic analyses and the making of thin sections as well as analysed for chemistry on location using a handheld XRF instrument, with higher sampling and measurement density closer to the lithological contacts.

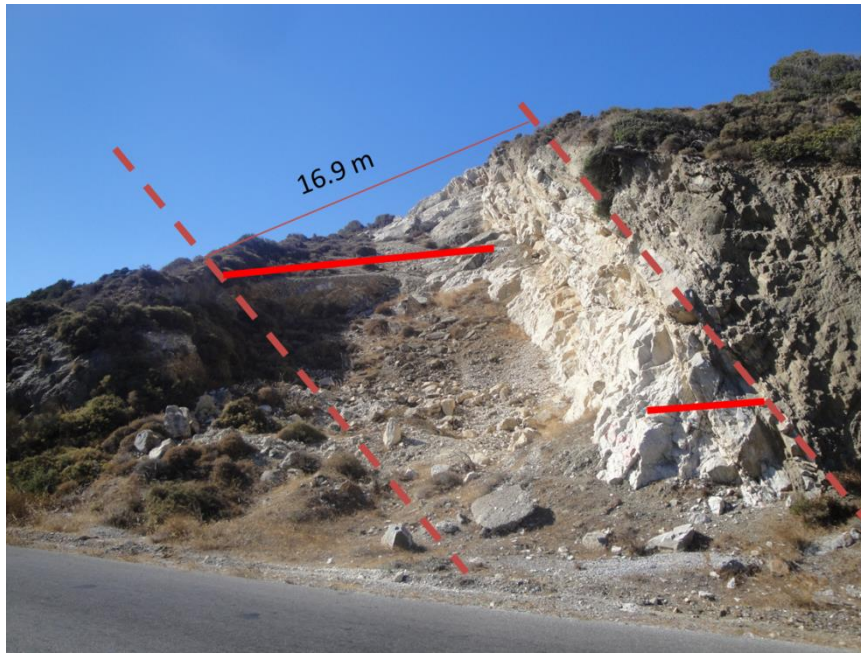


Figure 7 - Locality B with the constructed sampling profile. The dashed line indicate the thickness of the marble layer, the solid bright red lines indicate where the two segments of the profile were sampled and the thin red line show the actual thickness of the marble to which all data points have been corrected for.

XRF measurements

A handheld XRF DELTA Premium device (Olympus Innov-X) was used for in-situ elemental analyses in 113 points along the constructed profile. The instrument contains a 40W Rh anode tube X-ray excitations source and a silicone drift detector (SDD) with a resolution within the 150-170 eV range. The settings “Mining mode Plus” and “Soil mode” were used in combination to obtain the widest spectrum of elements. The different modes use different normalization algorithms, making Mining mode Plus suitable for calculating concentrations of major elements with concentrations above 0.5 wt% while Soil mode is best used for trace elements with concentrations less than 1wt%.

Since XRF is a surface measurement, care was taken to make measurements on fresh and smooth surfaces to avoid any contamination from surface weathering products and eliminate air between the rock and the analysing window of the instrument.

Quality control of the data was made by calibrating against chemical compositions obtained by ICP-MS analysis of 20 rock samples sent to ActLabs (Vancouver).

The results of elemental analyses are presented in Appendix B.

Stable isotopic analysis

A total of 68 calcite samples from Locality B were collected and analysed for oxygen and carbon isotopic compositions in the Stable Isotope Laboratory (SIL) at the department of geological sciences at Stockholm University. Six schist samples contained enough calcite for accurate analysis. Any weathered surface was removed from the ca. 3 cm³ samples before milling in a tungsten shatter box. Ca 0.2 mg of each sample were placed in vials and dried in 90°C before 100µl concentrated H₃PO₄ was injected with the vial in horizontal position, not allowing reaction between the acid and sample. Each vial was then placed in a flush rack and flushed with helium gas (100ml/min) for 10 minutes before turning the vial to a vertical position letting the acid react fully with the sample. The samples were introduced to a Gasbench II connected to a MAT 253 mass spectrometer, both from ThermoScientific. The samples were run against IAEA-CO-1, IAEA-CO-8 and NBS18 internal standards. Errors on individual calcite analyses are ±0.15‰ for δ¹⁸O and ±0.07‰ for δ¹³C.

The delta notation is given by the convention

$$\delta = \frac{R_{sample} - R_{standard}}{R_{standard}} 1000 \quad (29)$$

where R_{sample} is the measured isotopic ratio of the sample and $R_{standard}$ is the isotopic ratio of a standard. Oxygen isotope values are given relative to the SMOW-standard (Standard Mean Ocean Water) and carbon isotope values are given relative to the PDB-standard (Pee Dee Belemnite).

The results of the stable isotopic analyses are presented in table 1.

Results

Rock chemistry

All results from XRF measurements are presented in Appendix B.

Chemical profiles across the marble layer are normalized to Zr which is considered immobile during fluid infiltration (figure 8). The concentration of Zr in the marble is uniform at around 0.004% or 40 ppm while sharply increasing to 0.010 – 0.017% or 100-170 ppm in the adjacent schist. The immobility of Zr is explained by the very low solubility of Zircon (which is the main source of Zr) in typical metamorphic fluids (Ayers and Watson, 1991).

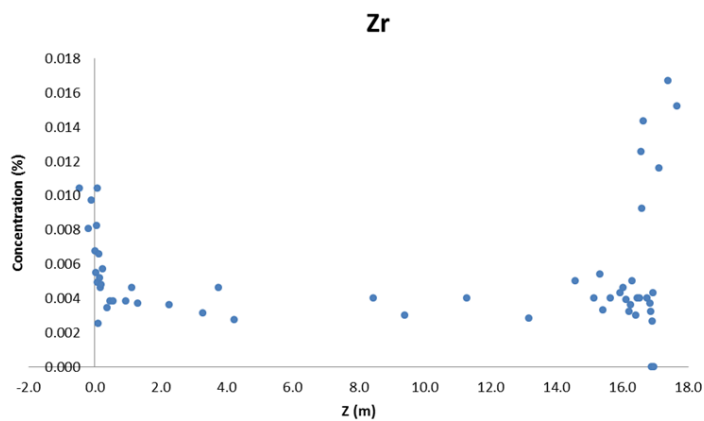


Figure 8 - Zirconium concentration profile across the marble layer at Locality B, obtained from XRF measurements. The difference in concentration between the schist and marble lithologies is distinct with a sharp increase directly at the lithological contacts witnessing of the immobility of Zr in metamorphic fluids.

Most elements have relatively uniform concentration ratio profiles in the interior of the marble layer. There are however, clear patterns of alteration in proximity of the lithological contacts including mass gain of Al, Fe, K, Si and Sr and mass loss of Ca (figure 9). Note that the number of data points close to the upper boundary region are twice as many compared to at the lower region, making it appear as though some of the elements have profiles looking more “right-skewed” than they are.

The high concentrations of Si, Al and Fe in the marble close to the upper lithological contact is likely an effect of infiltration by a retrograde fluid forming layer parallel calc-silicate assemblages (Baker et al., 1989).

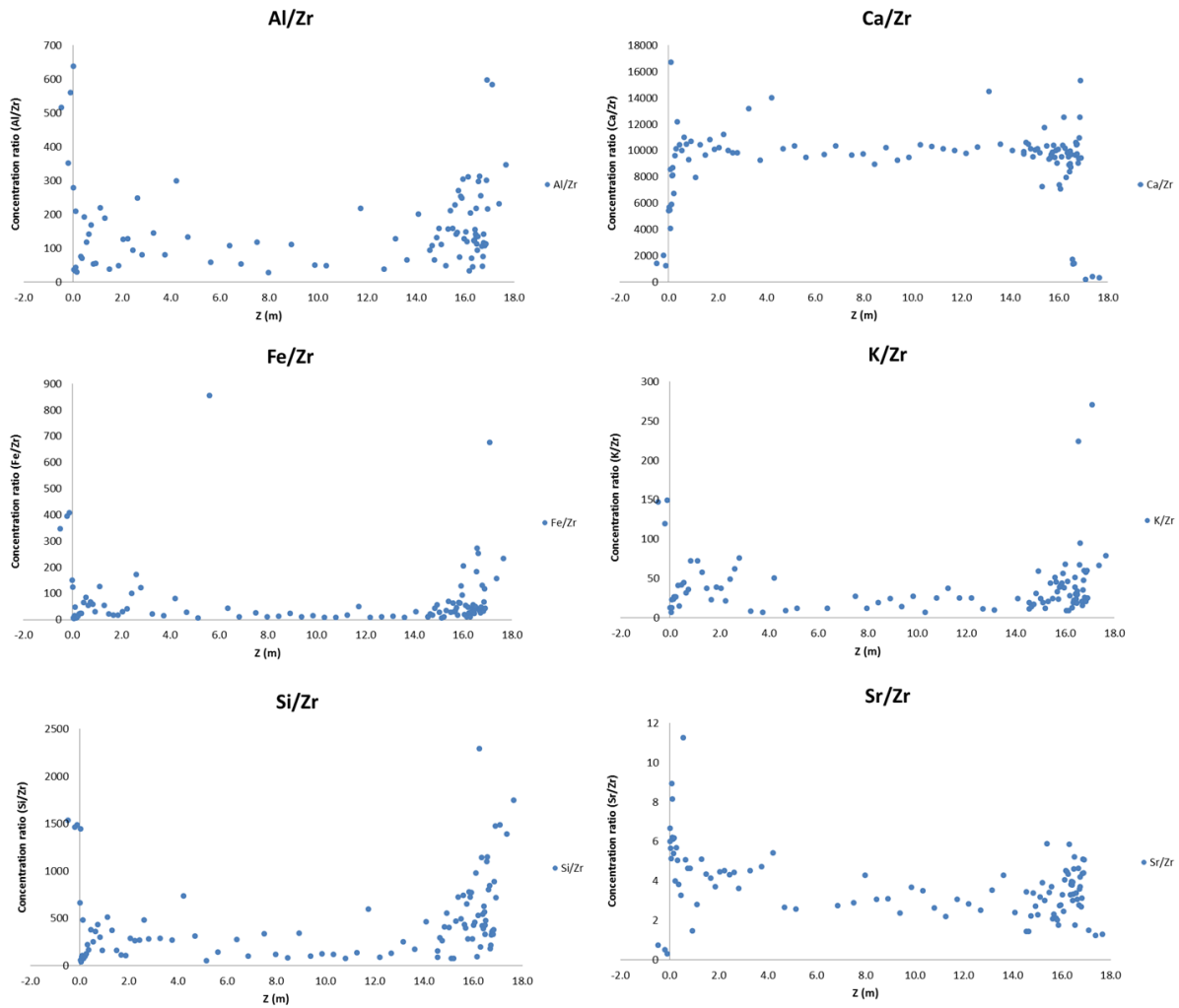


Figure 9 - Chemical profiles obtained from XRF measurements across the marble layer at Locality B. All profiles are given as concentration ratios, normalized to the concentration of Zr.

The elements which are enriched at the lower contact generally have concentrations that are higher in the adjacent schist compared to the marble. The fluid which is in equilibrium with the schist will re-equilibrate as it infiltrates the marble and either deposit elements (when concentration in schist is higher than the concentration in the marble) or strip the rock of elements (when the concentration in the schist is less than in the marble). This appears to be true for Si, Al, K, and Fe which are enriched in the marble at the lower lithological contact, and for Ca which is depleted from the boundary layer close to the contact. Sr stands out from this reasoning by having lower concentrations (40 ppm) in the schist compared to the marble (140 ppm) but still depositing high amounts of Sr into the marble.

Isotopic profiles

Oxygen and carbon isotopic profiles across the marble at Locality B are presented in table 1 and illustrated in figures 10 and 11. The interior of the marble has a $\delta^{18}\text{O}$ composition of 27‰ and a $\delta^{13}\text{C}$ composition of 1.5‰ which are typical for marine sediments (Hoefs, 2009). The oxygen isotopic profile displays a clear pattern of alteration with a 70 cm wide boundary layer at the lower lithological contact, displaying a decrease in $\delta^{18}\text{O}$ from 27‰ to 17-20‰. The upper boundary layer is much more narrow and sharp, although somewhat obfuscated by one of two larger dips in $\delta^{18}\text{O}$ that are visible along the profile. These dips are centred around 3.5 and 15 meters and have their lowest $\delta^{18}\text{O}$ values reaching 22 and 19‰ respectively. The lowest $\delta^{18}\text{O}$ value is as low as 10‰ and can be found in the schist above the upper lithological contact. The oxygen isotopic distribution varies within the lithologies and do not correlate particularly well to lithological variations.

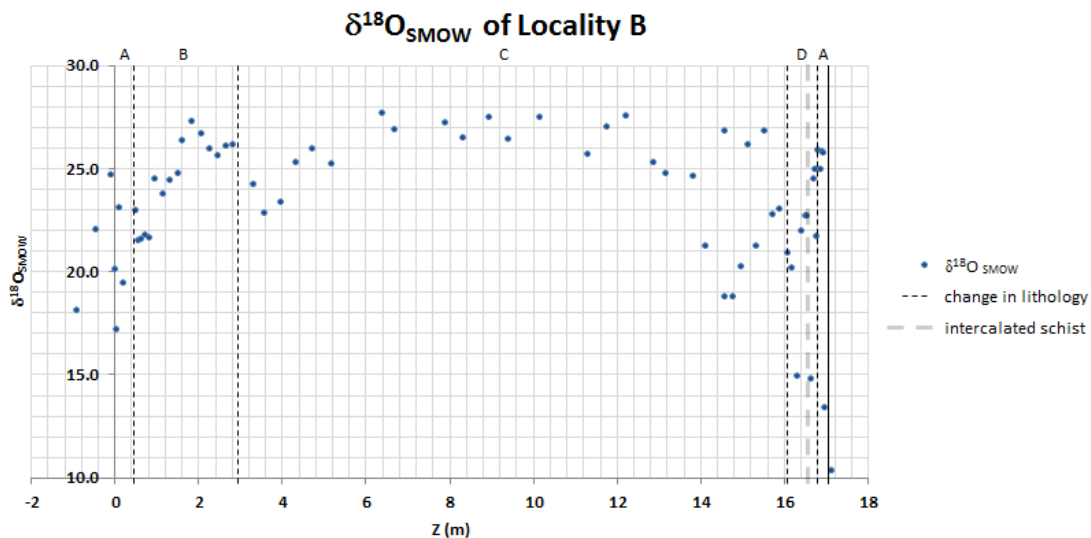


Figure 10 - Distribution of oxygen isotopic composition across the profile at Locality B. The lithological contacts between the schist and marble are located at 0m and 16.9 m and are marked with solid lines. The dashed black lines corresponds to changes in lithology within the marble which are represented by capital letters A-D, where A is the coarse white calcite marble, B is the hematite-margarite bearing brown marble, C is the light grey marble and D is the dark grey marble. The light grey dashed line represents the intercalated schist with a thickness approximately the width of the line.

The carbon isotopic profile show large variations in $\delta^{13}\text{C}$ in proximity to the lithological contacts with values reaching as low as -10‰ in the calcites of the schist at the lower contact and -5‰ in the calcite of the schist above the upper contact. Variations in $\delta^{13}\text{C}$ correlate to changes in lithology, with a distinct lowering of $\delta^{13}\text{C}$ to ca. -2.5‰ coinciding with the hematite-margarite lithology the first few meters of the profile compared to interior values of ca. +2‰ coinciding with the light grey marble. At the start of the dark grey marble close to the upper contact the $\delta^{13}\text{C}$ decreases to ca. -1.5‰ before sharply increasing to +2‰ again in the narrow band of white marble close to the upper lithological contact. Also the lower contact region consists of a 30 cm band of white marble with a $\delta^{13}\text{C}$ value of +2‰.

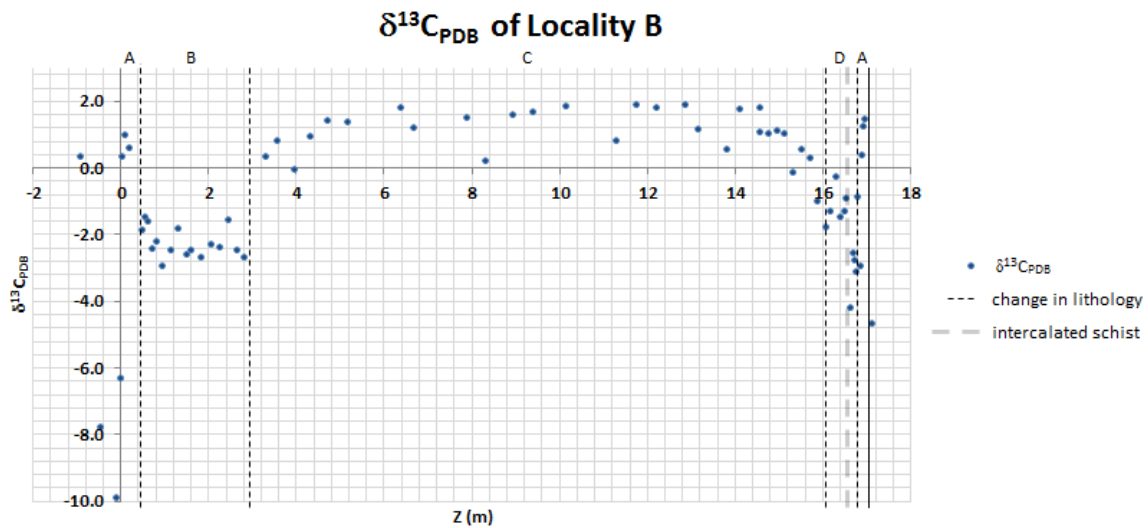


Figure 11 - Distribution of carbon isotopic composition across the profile of Locality B. Changes in lithology corresponding to capital letters A-D as in figure 10. There is an evident correlation between changes in lithology and variations in $\delta^{13}\text{C}$ across the profile. The coarse white calcite (A) closest to both contacts with the schist have positive $\delta^{13}\text{C}$ reaching +1‰ in the lower sequence and +1.5‰ in the upper. The brown marble (B) has a negative isotopic composition of ca. -2.5‰ while the light grey interior of the profile (C) have values reaching slightly higher than +1.5‰. The $\delta^{13}\text{C}$ within the dark marble is negative with decreasing values from around 0 to ca. -5‰ before becoming positive again in the narrow band of white marble close to the upper contact. The schists adjacent to the upper and lower contact have negative $\delta^{13}\text{C}$ values of -4‰ and -10‰ respectively.

Z	$\delta^{18}\text{O}_{\text{SMOW}}$	$\delta^{13}\text{C}_{\text{PDB}}$	Comments	Z	$\delta^{18}\text{O}_{\text{SMOW}}$	$\delta^{13}\text{C}_{\text{PDB}}$	Comments
(m)	(‰)	(‰)		(m)	(‰)	(‰)	
-0.94	18.17	0.36		9.40	26.46	1.68	
-0.47	22.05	-7.77	Schist	10.15	27.49	1.88	
-0.09	24.72	-9.88		11.28	25.72	0.82	
-0.02	20.14	-6.31		11.75	27.07	1.89	
0.02	17.20	0.37		12.22	27.60	1.83	
0.09	23.13	1.00	white coarse cc	12.87	25.29	1.88	
0.19	19.51	0.59		13.16	24.76	1.16	
0.47	22.97	-1.84		13.81	24.64	0.58	
0.56	21.53	-1.47		14.10	21.25	1.75	
0.61	21.61	-1.61		14.57	26.82	1.83	
0.70	21.81	-2.40		14.57	18.84	1.08	start of segment two of profile
0.80	21.68	-2.18		14.75	18.83	1.03	
0.94	24.50	-2.94		14.94	20.30	1.13	
1.13	23.82	-2.47	Brown marble with layer parallel hematite and margarite	15.13	26.17	1.06	
1.32	24.48	-1.81		15.32	21.29	-0.12	
1.50	24.82	-2.59		15.50	26.83	0.55	
1.60	26.36	-2.46		15.69	22.80	0.30	
1.83	27.29	-2.67		15.88	23.06	-0.98	
2.07	26.74	-2.27		16.07	20.91	-1.76	
2.26	25.98	-2.39		16.16	20.18	-1.27	
2.44	25.69	-1.54		16.30	14.99	-0.26	Dominantly dark grey marble
2.63	26.11	-2.45		16.39	22.03	-1.47	
2.82	26.18	-2.67		16.48	22.72	-1.29	
3.29	24.23	0.34		16.54	22.75	-0.89	
3.57	22.89	0.82		16.61	14.80	-4.18	intercalated schist
3.95	23.37	-0.03		16.70	24.54	-2.55	
4.32	25.30	0.96		16.74	25.01	-2.74	Dominantly dark grey marble
4.70	25.97	1.41		16.76	21.72	-3.11	
5.17	25.24	1.39	dominantly light grey marble with bands of darker grey marble	16.80	25.92	-0.87	
6.39	27.72	1.80		16.85	24.99	-2.92	
6.67	26.92	1.23		16.90	25.84	0.37	white marble
7.89	27.25	1.52		16.91	25.82	1.28	
8.32	26.49	0.23		16.96	13.41	1.49	Schist
8.93	27.51	1.60		17.10	10.38	-4.65	

Table 2 – $\delta^{18}\text{O}$ and $\delta^{13}\text{C}$ distribution across the marble layer at Locality B including comments on lithology

Discussion

Best-fit parameterization

The computer program DataFit (Oakdale Engineering) is used to fit equation (10) and (27) to geochemical and isotopic data from Locality B on Naxos by nonlinear regression. The goal of the nonlinear regression is to determine the best-fit parameters for the models by minimizing a chosen merit function:

$$\chi^2 = \sum_{i=1}^n \left[\frac{\delta_{z_i} - f(z_i)}{\sigma_i} \right]^2 \quad (30)$$

where δ_{z_i} is the value of the measured isotopic or elemental composition and $f(z_i)$ is the value of the model function in the i^{th} data point respectively. σ_i is the standard deviation or measurement error of the i^{th} data point. The process of merit function minimization is an iterative approach which minimizes the sum of squares of the distances between the sample data points and the model curve. The value of χ^2 is small when the agreement between the data and model curve is good.

Fitting data to the pinned boundary model

The Pinned boundary model allows fitting of both lithological contacts simultaneously and can therefore take all data points across the profile into consideration. Regression variables are the initial concentration of the geochemical tracer in the schist (C_1), the initial concentration of the tracer within the marble (C_2), the Peclet number (N_{Pe}) describing the importance of advection relative diffusion and the dimensionless time (t'). n in the solution (equation 10) is chosen as 200.

Fitting data to the linear kinetics exchange model

Equation (27) cannot handle both lithological contacts at the same time. The linear kinetics exchange model is therefore fitted to data points in the lower contact region, from where the prograde fluid has infiltrated, and 11 meters into the marble. The integral in equation (27) is solved using the composite Simpson method with $n=100$. The regression variables are the

initial concentration of the geochemical tracer in the schist (C_1), the initial concentration of the tracer within the marble (C_2), the Damhöhler number (N_D) and the displacement of the geochemical front in meters (Z_{GF}).

Results from model fitting

The best-fit estimates of the independent variables for the pinned boundary and linear kinetic exchange models have been obtained for oxygen isotopic data as well as for Fe, Al and Sr elemental data and are presented below in table 2 and figures 12 – 14. All error estimates are given as 1σ (68% confidence interval).

The goodness-of-fit of the models is compared by their respective R^2 -value, or coefficient of determination, which is a statistical measure of how well the regression line approximates the real data points. The R^2 -value is defined as:

$$R^2 = 1 - \frac{SS_{RES}}{SS_{TOT}} \quad (31)$$

where SS_{RES} is the residual sum of squares defined as:

$$SS_{RES} = \sum_i (y_i - f_i)^2 \quad (32)$$

and SS_{TOT} is the total sum of squares which is equivalent to the sample variance:

$$SS_{TOT} = \sum_i (y_i - \bar{y})^2 \quad (33)$$

y_i is the sample value and f_i the modelled value of the i^{th} data point respectively, and \bar{y} is the mean value of the sample data. The R^2 value ranges between 0 and 1, and approaches 1 as the goodness-of-fit increases. An R^2 of 1 indicates that the regression line perfectly fits the data.

	$\delta^{18}\text{O}$ (‰)	$\delta^{18}\text{O}$ (‰)	Al (%)	Fe (%)	Sr (ppm)
Transport model	Pinned Boundary	Linear Kinetic exchange	Linear Kinetic exchange	Linear Kinetic exchange	Linear Kinetic exchange
	<i>both contacts</i>	<i>lower contact</i>	<i>lower contact</i>	<i>lower contact</i>	<i>lower contact</i>
No. of data points	65	38	37	46	46
σ	3.45	1.41	0.44	0.52	83.4
R^2	0.16	0.68	0.62	0.24	0.56
Best-fit parameter					
C_1	16.95 ± 1.72	19.69 ± 1.07	1.86 ± 0.37	2.06 ± 0.92	454.35 ± 46.53
C_2	25.00 ± 0.58	26.02 ± 0.29	0.42 ± 0.08	0.23 ± 0.14	136.91 ± 16.86
N_D		3.35 ± 0.59	5.66 ± 0.02	2.71 ± 0.08	1.67 ± 0.01
Z_{GF}		0.72 ± 0.13	0.04 ± 0.008	0.02 ± 0.03	0.29 ± 0.11
N_{Pe}	11.68 ± 19.67				
t'	0.00064 ± 0.0006				

Table 3 – Estimated values of best-fit parameters from model-fitting of oxygen isotopic composition, Al, Fe and Sr elemental data from the sampled profile. The Linear kinetic model is fitted to data ranging from the lower lithological contact to 11 meters into the marble. Error estimates are given as 1σ (68% confidence interval).

Oxygen isotopic profile

The oxygen isotopic data could be fitted to both models and model plots are illustrated in figures 12 and 13. The estimated analytical error of the fit is $\pm 3.45\%$ for the pinned boundary model and $\pm 1.41\%$ for the linear kinetic model and R^2 -values are 0.16 and 0.68 respectively.

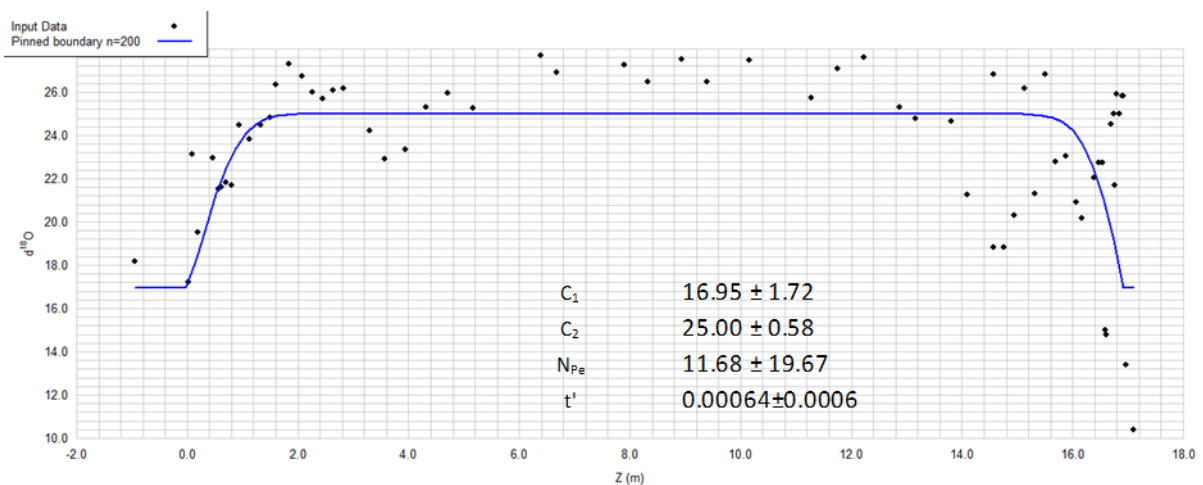


Figure 12 - Model plot for oxygen isotopic profile fitted to the pinned boundary model.

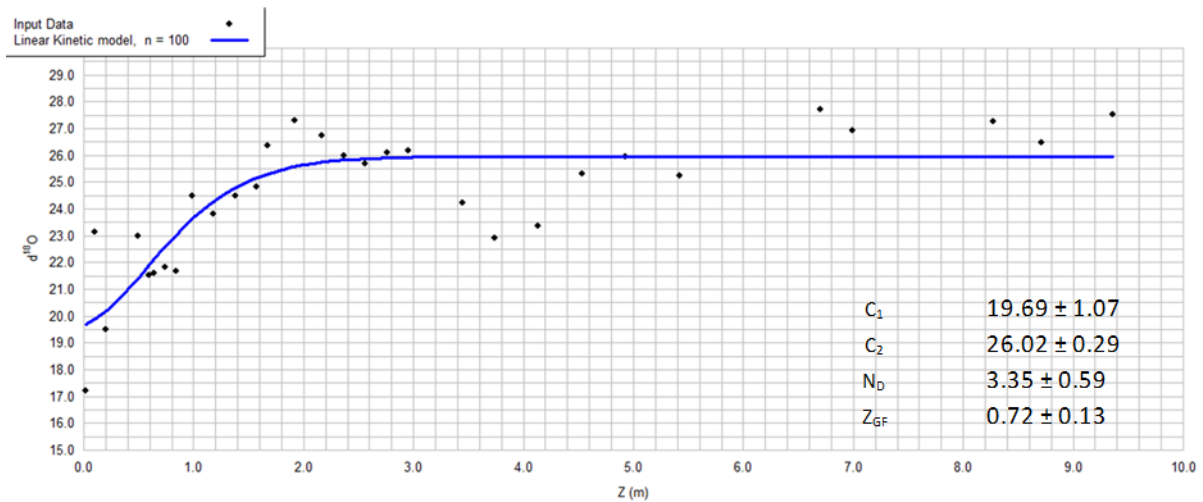


Figure 13 – Model plot for oxygen isotopic profile fitted to the linear kinetic model

The results from model curve fitting of the oxygen isotopic profile clearly shows that the linear kinetic model provides the best fit to the data. The poor fit to the pinned boundary model in this study compared to previous results by Bickle and Baker (1990) was expected. They obtain a standard error (σ) between the model curve and their data from Locality B of ± 0.23 compared to ± 3.45 in this study (there is no reported R^2 value for comparison). However, their fit includes only 11 data points close to the lower lithological contact (2 meters into the marble). By that they avoid fitting most of the scatter in the data, including the two clusters of data points with anomalously low $\delta^{18}\text{O}$. The addition of 54 data points (total of 65) over the entire marble layer, have shown that the model in fact does not provide a particularly good fit. This implies that previous conclusions drawn about the fluid infiltration event needs to be revised. Conclusions made regarding the assumption of grain-scale equilibrium between the marble and the fluid may not be valid. The better fit by the linear kinetic model implies instead that the fluid was transported advectively through evenly spaced micro-cracks and that the broadening of the front was caused by diffusion into the wall rock perpendicular to the cracks.

Best-fit estimates from model fitting to the linear kinetic exchange model provides a C_1 of $19.69 \pm 1.07\text{‰}$ corresponding to the $\delta^{18}\text{O}$ that the calcite in the marble would have in equilibrium with the fluid phase in the schist, a C_2 value of $26.02 \pm 0.29\text{‰}$ corresponding to the protolith composition in the interior of the marble layer, a dimensionless Damköhler number of 3.35 ± 0.59 and a position of the oxygen isotopic front at 0.72 ± 0.13 meters.

Carbon isotopic profile

The carbon isotopic profile was not fitted to any of the tracer transport models. What needs to be considered are that (1) the $\delta^{13}\text{C}$ distribution closely relates to primary lithological features and (2) that small amounts of graphite present in the schist and marble locally but drastically lowers the $\delta^{13}\text{C}$ values.

Recent graphitic clastic sediments have an isotopic composition of ca -25‰ (Kreulen and Van Beek, 1983) but graphites in metamorphic rocks often have higher values caused by isotopic exchange between the calcite and graphite. This exchange is often partial and the calcites in Naxos marbles are believed to be in disequilibrium with the graphite (Kreulen and Van Beek, 1983). It is enough that small quantities of graphite are present to drastically lower $\delta^{13}\text{C}$ of the original marine values of the calcite (Baker et al., 1989).

The correlation between $\delta^{13}\text{C}$ values and lithology, and effects on $\delta^{13}\text{C}$ composition by the presence of graphite indicate that the fluid was water-rich and did not contain high enough amounts of CO_2 to create an overprint on the original $\delta^{13}\text{C}$ compositions. This implies that the current distribution of $\delta^{13}\text{C}$ across the marble band was not created by the infiltrating fluid, and should therefore not be fitted to a model which describes such a phenomenon.

Element profiles

Elements that exhibit geochemical fronts have been fitted to the linear kinetics exchange model. These elements are Al, Fe and Sr. Analytical errors of the fits are $\pm 0.44\%$ for Al, $\pm 0.52\%$ for Fe and ± 83.4 ppm for Sr. Figure 14 illustrate the model plots.

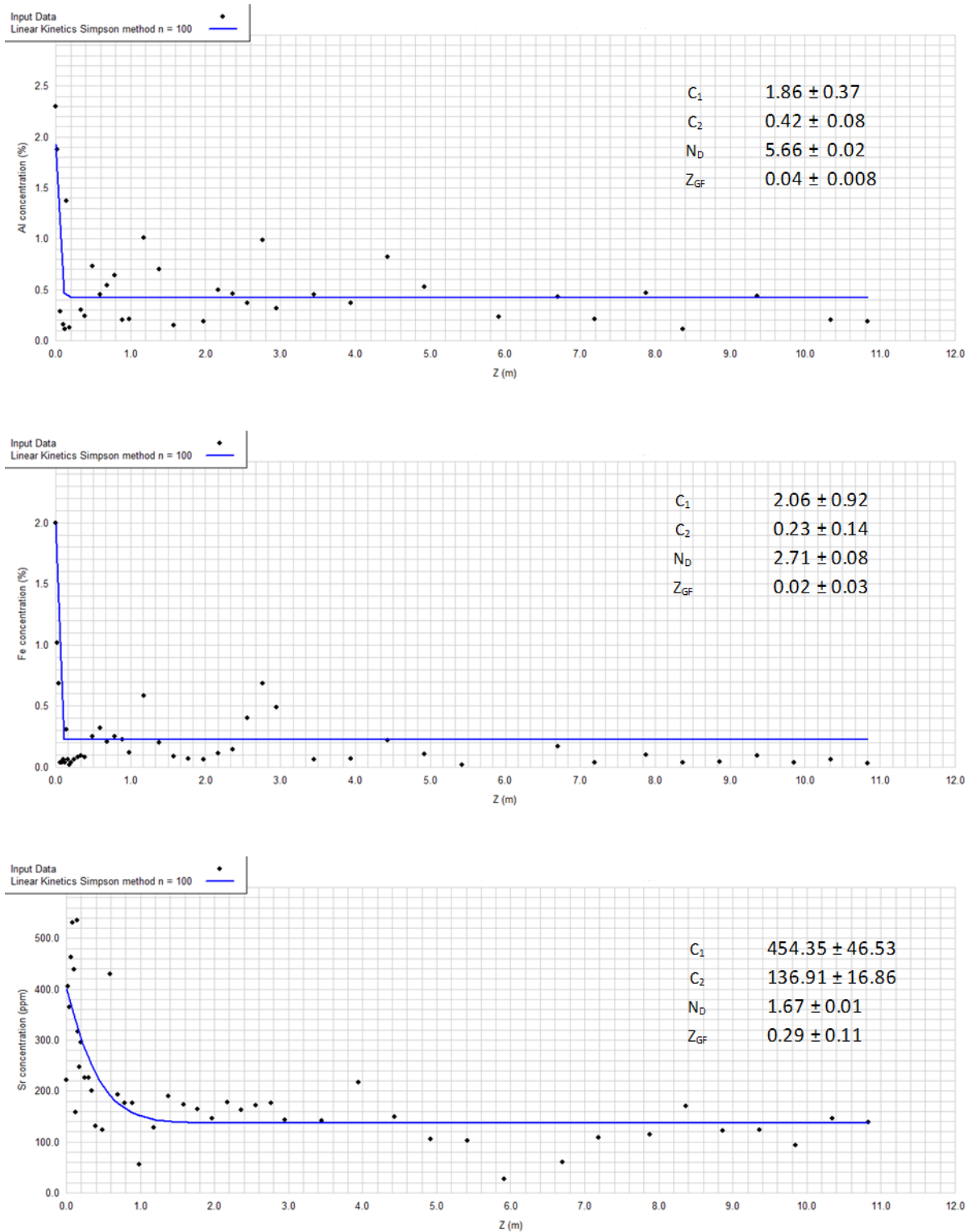


Figure 14 – Model-fits of the element data to the linear kinetic exchange model. The uppermost plot illustrates the fit of the model to Al concentration, the middle to Fe concentration and the lowermost to Sr concentration. All profiles extend 11 meters into the marble from the lower lithological contact. Note the wider boundary layer of Sr compared to Fe and Al.

The obtained best-fit estimates of the C_1 parameter for each of the elements describe the hypothetical concentration that the calcite of the marble would have in equilibrium with the fluid in the schist. This value together with the front propagation distance and the calculated time-integrated fluid flux can be used to estimate the concentration of the fitted elements in the infiltrating fluid.

Volumetric solid-fluid partition coefficient

The solid-fluid partition coefficient is the ratio between the concentration of the geochemical tracer or tracer carrier (oxygen atoms in the case of ^{18}O) in the solid and its concentration in the fluid. K_v essentially describes how far a geochemical will be transported with the fluid and can be compared to the *retardation factor* used in chromatography. If the tracer is partitioned into the fluid phase it will be transported further than if it is more likely to partition into the rock. Figure 14 suggests that Fe and Al are more readily partitioned into the rock than Sr, which has a much wider boundary layer and has been transported further with the fluid.

The partition coefficient for oxygen can be estimated easily since oxygen is abundant in both the solid and fluid. The solid-fluid partition coefficient by volume, K_v is defined as:

$$K_v = \frac{\rho_s C_s}{\rho_f C_f} \quad (34)$$

where ρ_s is the density of calcite (2700 kg/m^3) and ρ_f the density of the fluid (assumed hereon as pure water, 1000 kg/m^3), C_s is the concentration of oxygen in the calcite ($\sim 0.48\%$) and C_f the concentration of oxygen in H_2O (~ 0.89).

K_v for oxygen is calculated to 1.46

Duration of fluid infiltration

The duration of the fluid infiltration event associated with the Miocene metamorphic event has previously been estimated as ranging between 7000 – 0.7 Ma (Bickle and Baker, 1990). This estimate was calculated with equation (4) used to transform the time to the non-dimensional variable t' in the pinned boundary model. Since it was established by best-fit of

the oxygen data that the pinned boundary model did not provide a satisfactory fit the duration of the infiltration event calculated from it might not be accurate.

The rate-limiting process of fluid-solid exchange in many metamorphic settings is likely transverse diffusive transport in either the fluid or solid phase (Bickle, 1992). This is especially true when the fluids are channelled through cracks. Equation (22) defines the Damköhler number as the rate of exchange between the fluid and the solid along a distance h , divided by the velocity of the fluid flow. If h is defined as the fluid infiltration distance (ωt) the equation can be rewritten as:

$$N_D = \kappa t \quad (35)$$

Equation (34) implies that the duration t of the fluid infiltration event can be estimated with the Damköhler number, N_D and the exchange rate constant, κ .

Provided that the front propagation is limited by diffusion into the wall rock, the exchange rate of the transverse diffusion between the fluid-filled cracks the wall rock may be approximated by the rate constant, κ , from equation (12) of the linear kinetic model. Bickle (1992) gives the expression of κ as:

$$\kappa = \frac{\pi^2 D_{eff}}{K_v 4B^2} \quad (36)$$

where B is half the spacing between the fluid conduits and D_{eff} describes the effective diffusivity of the system (equation 2). Lewis et al. (1998) showed by cathodoluminescence analysis of the marble at Locality B that the grain boundaries acted as micro-cracks making B half the grain diameter. The grain size differs greatly across the profile but is quite coarse close to the lower lithological contact where the fluid has infiltrated. Bickle and Baker (1990) use an average grain diameter of 1mm giving a value for B of 0.0005m.

Since the fluid can be seen as moving advectively in the z -direction on each side of a calcite grain, the slowest mechanism governing the displacement of the isotopic front will be diffusion through the solid phase. Substituting D_{eff} to D_s (the diffusivity constant of oxygen through the solid calcite) and using the value of $3.15 \times 10^{-19} \text{ m}^2/\text{s}$ obtained experimentally by Farver (1994) for 600°C and pressures of 1MPa, and the calculated 1.46 for K_v , equation (36) yields an exchange rate κ of $9.46 \times 10^{-13} \text{ s}^{-1}$.

Using the best-fit value of 3.35 ± 0.59 for the Damköhler number, equation (35) gives the time it would take to displace the oxygen isotopic front 0.72 ± 0.13 meters into the marble by transverse diffusion into the solid crystal network of the wall rock, as approximately $113\,000 \pm 20\,000$ years.

Fluid flux calculations

The displacement of the oxygen isotopic profile can be used to estimate the magnitude of the infiltrating fluid. Provided that h in equation (14) is chosen as the fluid penetration distance (ωt) the expression for calculating the time-integrated fluid flux ($\omega \varphi t$) is given by:

$$\omega \varphi t = z_{GF} K_v \quad (37)$$

where Z_{GF} is the displacement of the oxygen isotopic front in meters, obtained from model fitting to the linear kinetic model.

Expression (37) gives a time-integrated fluid flux of $1.05 \pm 0.02 \text{ m}^3/\text{m}^2$ which is in agreement with previous studies (Bickle and Baker, 1990). Given that the rate constant in equation (12) is transport limited, the time-averaged fluid flux (time-integrated fluid flux divided by the duration obtained from equation 35) is calculated to $2.98 \times 10^{-13} \pm 5.28 \times 10^{-14} \text{ m}^3/\text{m}^2/\text{s}$. This is one order of magnitude larger than the time-averaged fluid flux obtained by data-fitting to the pinned boundary model (Bickle and Baker, 1990).

Pelitic rocks are considered as one of the most H_2O -rich sedimentary rocks in the crust with approximately 5wt% chemically bound H_2O (Walther and Orville, 1982). To produce a fluid volume of $1.05 \pm 0.02 \text{ m}^3/\text{m}^2$ would require only a few meters of the rock to dehydrate. The schist sequences on Naxos are several hundreds of meters thick, making it very likely that most of the fluid is channelled through the more permeable schist, with only a small fraction being transported through the nearly impermeable marbles.

Composition of the infiltrating fluid

The C_1 parameter obtained from model-fitting equals the pinned concentration the marble has at the lower lithological contact. This concentration is the hypothetical concentration the marble has in equilibrium with the fluid phase infiltrating from the adjacent schist. Knowing

the fractionation factor, α , between the calcite and fluid under appropriate metamorphic conditions allows the calculation of the isotopic composition of the infiltrating fluid.

Experimental results by O'Neil et al. (1969) give the fractionation of oxygen isotopes between water and calcite as:

$$1000 \ln \alpha = 2.78(10^6 T^{-2}) - 3.39 \quad (38)$$

where α is the fractionation factor and T the temperature in degrees Kelvin. However, this expression is only accurate for temperatures reaching 550°C which is almost one hundred degrees less than the peak metamorphic temperatures at Locality B. However, the fractionation of oxygen isotopes between water and calcite is small and decreases with increasing temperatures and for the purpose of this study equation (37) provides sufficient results. Using a temperature of 600°C (873°K) The fractionation is as small as 0.25‰ meaning that with a best-fit estimate of C_1 of $19.69 \pm 1.07\text{‰}$ the oxygen isotopic composition of infiltrating fluid was 19.44‰. This is considerably higher than previously reported values of 12-16‰ (Baker et al., 1989; Bickle and Baker, 1990) but still in the range of typical metamorphic fluid derived from dehydration of a pelite (Hoefs, 2009).

Calculations of element concentrations of the fluid

The obtained values for C_1 and Z_{GF} from model-fitting of the element data can be used together with the calculated time-integrated fluid flux to estimate a concentration of the element in the infiltrating fluid. Equation (34) and (37) are re-written to the form:

$$C_f = Z_{GF} \frac{\rho_s C_1}{\rho_f \omega \phi t} \quad (39)$$

where Z_{GF} and C_1 are values for each specific element, and $\omega \phi t$ is the time-integrated fluid flux obtained from the oxygen isotopic profile. What equation (39) essentially states is that if the concentration of the element that has been deposited in the rock over a certain distance is known, and the volume of fluid which has passed through the area is known, it is possible to calculate the concentration of the element in the fluid.

Using equation (38) and values obtained from model-fitting (table 2) estimated concentrations of the fluid are 2000 ± 3900 ppm for Al, 1100 ± 1700 ppm for Fe and 341 ± 134 ppm for Sr. As seen in these results the standard deviations are large especially for Al and Fe as a consequence of the error propagation which increase each step of the calculations. However the calculated concentrations of the fluid in equilibrium with the marble at the lithological contact allow interpretations of the origin of the infiltrating fluid. Yardley (2005) presents element concentrations for typical geological fluids and these values all fall in the range of a metamorphic fluid. The concentrations are considerably lower than would be expected if the fluid was derived from recrystallization of the underlying migmatite or intruding granodiorite bodies in the North West of Naxos.

The small volume of fluid that has infiltrated the marble in conjunction with the calculated element concentrations which have a metamorphic signature, strongly suggests that the fluid was derived from dehydration of the underlying schist.

Effects of retrograde fluid infiltration at Locality B

The Naxos marbles show signs of retrograde metamorphism in the form of calc-silicate assemblages and veins laying layer-parallel or crosscutting many higher grade marbles and dolomites (Rye et al., 1976; Baker et al., 1989; Baker and Matthews, 1994). The retrograde fluid was water-rich with a $\delta^{18}\text{O}$ composition of $\leq 10\text{‰}$ and $\delta^{13}\text{C}$ composition of about -4‰ (Baker et al., 1989). There are a few data points close to the upper lithological contact at Locality B having such low values in both oxygen and carbon isotopic composition indicating infiltration of the retrograde fluid. However, the marble at Locality B does not contain any crosscutting veins which are visible in other high grade localities on the island (c.f. Baker and Matthews, 1994) but show only narrow streaks of retrograde assemblages lying parallel to primary layering.

The retrograde fluid likely originated from the crystallising migmatite, giving it an igneous isotopic composition and elevated concentration of rock-forming elements. Calc-silicate assemblages are highly metasomatic and require mobility of Al, Si and possibly Fe and Mg, as well as loss of Ca (Ague, 2003). A concentration ratio diagram where the concentration of a measured element is normalized to its protolith concentrations can visualize gains or losses of elements which can aid in identifying regions affected by retrograde fluid infiltration.

Figure (15) illustrates the local gains and losses of Al, Fe, Si, Mg, Ca and Sr. The protolith

values of Al, Fe and Sr were obtained from model-fitting to the linear kinetic model (parameter C_2) while the protolith values for Mg, Si and Ca (which could not be modelled with good results) were chosen as the average concentrations of the specific element from the interior of the marble having protolith (marine carbonate) isotopic compositions (between 7 - 13 meters on the profile).

A concentration ratio of 1 means that the element has not been added or stripped from the rock by fluid interaction, and has the same concentration as it did in the protolith stage. Ca show little fluctuation along the profile and almost constantly has a ratio of 1. However the Ca concentration in the protolith and altered rock is very high (almost 40%) meaning it would take an increase to 80% in the altered rock just to show a small peak in the diagram. The very small fluctuations of Ca that are seen in figure (15) should therefore not be neglected. The Ca concentration ratio is included in the figure for two reasons, (1) small fluctuations may be indicative of metasomatic processes where Ca is removed in favour of growth of calc-silicates, and (2) because it graphically helps assessing the gain or loss the other elements in the diagram; for most cases (where the Ca ratio is close to one) a concentration ratio under the Ca-line (black line in figure 15) means loss of that particular element, while a concentration ratio plotted above the Ca-line is indicative of mass gain of the element. Note that the figure contains concentration ratios, especially of Mg, plotted as 0. This occurs in those data points which had concentrations lower than the detection limit of the XRF instrument, and does not necessarily imply that the rock does not contain any Mg in that point.

Figure (15) allows distinction between different processes that has altered the elemental composition across the profile. The first peaks of the plotted elements occur very close to the lower lithological contact (cm scale). Over the same distance as the elements Al, Fe, Si, Mg and Sr are heavily enriched (several hundred per cent relative the protolith) Ca is lost. This very narrow initial zone of alteration (wider for Sr) corresponds to deposition (or leaching in case of Ca) of the elements by the infiltrating prograde fluid.

The hematite-bearing marble between 0.5 and 2.9 meters contain three distinct peaks of Fe, Si and Al. Over the same distance there is a slight decrease in the Ca ratio meaning that these peaks could be derived from retrograde infiltration.

The interior of the marble is characterised by fairly homogeneous oxygen and carbon isotopic composition, as well as a relatively uniform elemental composition. At $z = 5$ meters there is one very high peak in Fe (almost 1500% increase relative unaltered rock composition).

However no other element plotted in figure (15) show any enrichment in this point. This Fe-peak is likely caused by analysis of a crack containing weathering products (Fe-oxides), which can be found in the hand specimen.

The region close to the upper lithological contact is characterised by heavy enrichments of Si, Fe, Al and mostly Mg. The peaks are accompanied by losses of Ca indicating alteration caused by fluid infiltration, and given the magnitudes of enrichment, infiltration of the retrograde fluid.

The shaded light grey areas of the profile in figure (15) are the two dips in $\delta^{18}\text{O}$ composition which can be seen in figure (10). Both areas each contain a peak of Si and Al. These two peaks are small compared to the retrograde peaks close to the upper contact and resemble the appearance of the other potentially primary peaks (more quartz-rich sedimentary layers) along the interior of the profile. Lowering of $\delta^{18}\text{O}$ within the profile has previously been attributed to the retrograde fluid infiltration (Bickle and Baker, 1990). However, by combining the estimates of fluid geochemical concentrations, isotopic compositions, and chemical alterations of the rock at these specific sites, with the conclusion that the linear kinetics exchange model (and associated fluid flow geometry) best describes the mechanism of tracer transport, these two sites of lowered $\delta^{18}\text{O}$ likely formed by channelling of the prograde fluid.

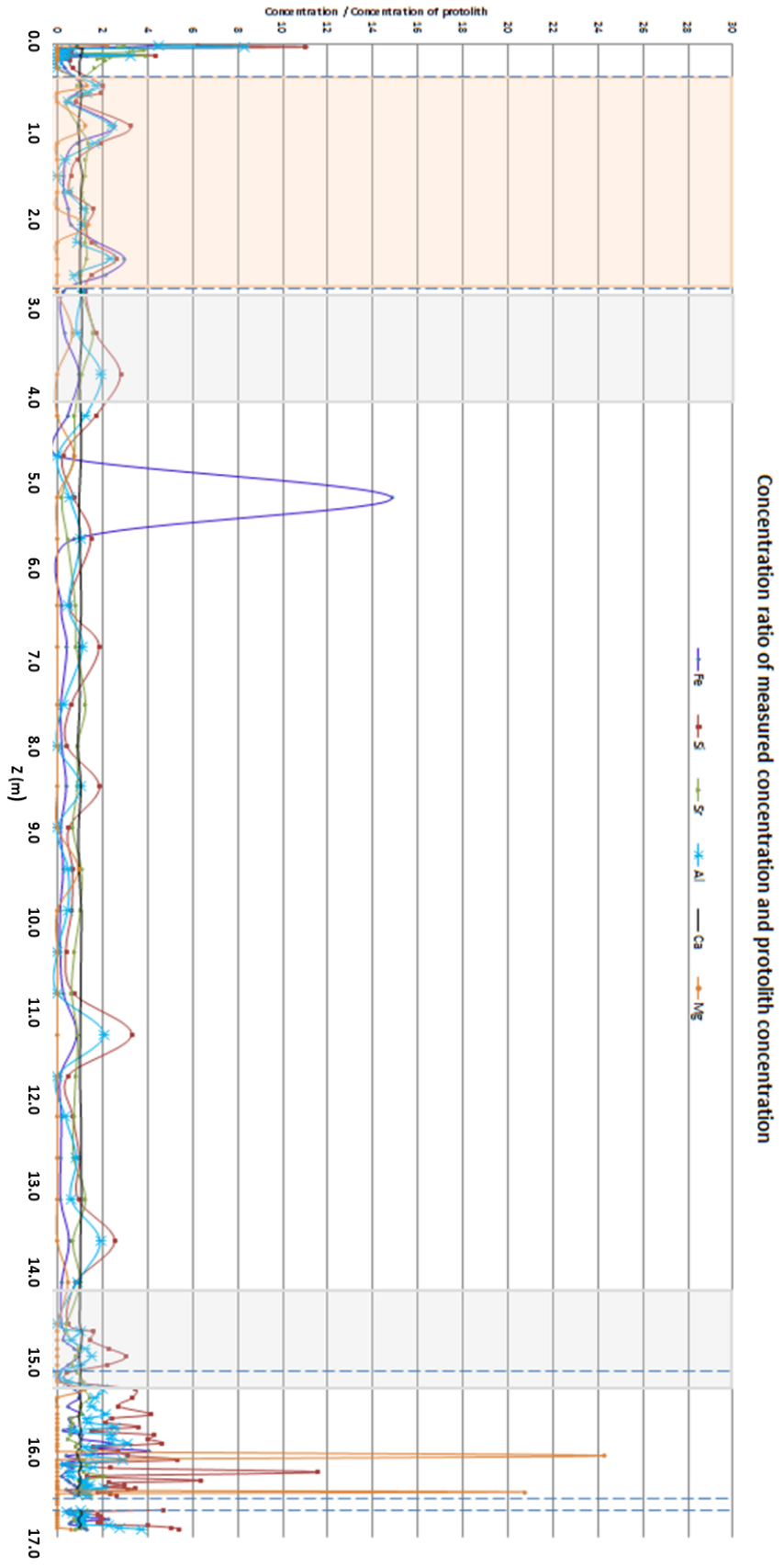


Figure 15 – Concentration ratio diagram of the marble, concentration of the measured element is normalised to concentration of the protolith. The dashed lines correspond to changes in lithology. The intercalated schist close to the upper contact is marked by a gap in the data (since no protolith values are obtained for the schist). The red field is marking the brown marble lithology containing hematite and margarite, and light grey fields mark dips in oxygen isotopic composition. See text for discussion.

Conclusions

Two one-dimensional transport models describing fluid transport through a porous medium have been fitted to oxygen isotope and geochemical data sampled across a 17 meters thick marble layer at Locality B on Naxos, Greece. The results indicate that previous conclusions drawn about fluid flow regime, transport mechanism and equilibrium conditions during the prograde fluid infiltration associated with the Miocene M2 metamorphic event, needs to be revised. The pinned boundary model, describing coupled advective-diffusive transport during grain-scale equilibrium does not provide a particularly good fit to the data (R^2 value of 0.16) compared to the linear kinetic exchange model (R^2 value of 0.68). These results imply that the isotopic boundary layer at the lower contact region likely formed as the prograde fluid was transported advectively through micro-cracks along grain boundaries with transverse diffusion into the calcite crystals limiting the exchange rate.

Best-fit estimates of fluid flow parameters obtained from fitting oxygen isotopic compositions to the linear kinetic model are used to calculate a time-integrated fluid flux of $1.05 \pm 0.02 \text{ m}^3/\text{m}^2$, a duration of the infiltration event of $113\,000 \pm 20\,000$ years and a time-averaged fluid flux of $2.98 \times 10^{-13} \pm 5.28 \times 10^{-14} \text{ m}^3/\text{m}^2/\text{s}$.

The carbon isotopic distribution across the marble at Locality B correlates well with lithological features and there are no distinct zones of alterations or a potential overprint by the prograde fluid. This is a strong indicator that the fluid was water-rich and did not contain enough CO_2 to alter the $\delta^{13}\text{C}$ across the profile.

The infiltrating fluid had a $\delta^{18}\text{O}$ value of ca. 19.5‰ and it is likely channelling of this fluid that has created the two distinct dips in $\delta^{18}\text{O}$ (19-22‰ compared to protolith values of 26.02 ± 0.29 ‰) visible along the profile. The calculated element concentrations of the infiltrating fluid are 2000 ± 3900 ppm for Al, 1100 ± 1700 ppm for Fe and 341 ± 134 ppm for Sr, also in the range of a metamorphic fluid. The small volume of fluid that has infiltrated the marble in conjunction with the calculated element concentrations and the isotopic composition of the fluid strongly suggests that the fluid was derived from dehydration of the underlying schist.

Acknowledgements

I would like to thank Alasdair Skelton for his supervision during this project, for supporting, challenging and encouraging me throughout the year. Also, thanks should be given to Elisabeth Däcker for supervision during field work on Naxos, Wen Zhang for assisting in the field, Dan Zetterberg for helping me with preparation of thin sections, Heike Siegmund for running my isotopic analyses, Per-Olof Åberg from the Natural History Museum for instructing me in the crushing lab, and to all of those who helped me carry my rock samples home to Sweden, Thank you! Last but absolutely not least, thank you to Daniel Töyrä who has spent countless hours teaching me the maths behind the models, and always being patient with my many questions.

References

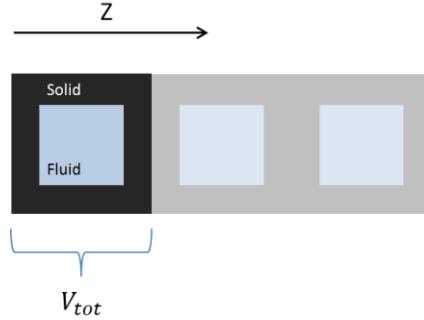
- Ague, J. J., (2003) Fluid infiltration and transport of major, minor, and trace elements during regional metamorphism of carbonate rocks, Wepawaug schist, Connecticut, USA, *American Journal of Science*, **303**, 753-816
- Avigad, D., Garfunkel, Z., (1991) Uplift and exhumation of high-pressure metamorphic terrains: the example of the Cycladic blueschist belt (Aegean Sea), *Tectonophysics*, **188**, 351-372
- Ayers, J. C., Watson, E. B., (1991) Solubility of apatite, monazite, zircon and rutile in supercritical aqueous fluids with implications for subduction zone geochemistry, *Philosophical Transactions of the Royal Society of London Series A*, **335**, 365-375
- Baker, J., Bickle, M. J., Buick, I. S., Holland, T. J. B., Mathews, A., (1989) Isotopic and petrological evidence for the infiltration of water-rich fluids during the Miocene M2 metamorphism on Naxos, Greece, *Geochimical et Cosmochimica Acta*, **53**, 2037-2050
- Baker, J., Matthews, A., (1994) Textural and isotopic development of marble assemblages during the Barrovian-style M2 metamorphic event, Naxos, Greece, *Contributions to Mineralogy and Petrology*, **116**, 130-144
- Baker, J., Matthews, A., (1995) The stable isotopic evolution of a metamorphic complex, Naxos, Greece, *Contributions to mineralogy and petrology*, **116**, 130-144
- Baumgartner, L. P., Rumble, D., (1988) Transport of stable isotopes , 1. Development of a kinetic continuum theory for stable isotope transport, *Contributions to Mineralogy and Petrology*, **98**, 417-430
- Bickle, M. J., (1992) Transport mechanisms by fluid flow in metamorphic rocks: oxygen and strontium decoupling in the Trois Seigneurs Massif – a consequence of kinetic dispersion? *American Journal of Science*, **292**, 289-316
- Bickle, M. J., Baker, J., (1990) Advective-diffusive transport of isotopic fronts: an example from Naxos, Greece, *Earth and Planetary Science Letters*, **97**, 78-93
- Bickle, M. J., McKenzie, D., (1987) The transport of heat and matter by fluids during metamorphism, *Contributions to Mineralogy and Petrology*, **95**, 384-392

- Buick, I. S., Holland, T. J. B., (1989) The P-T-t path associated with crustal extension, Naxos, Cyclades, Greece, *Geological Society, London, Special Publications*, **43**, 365-369
- Farver, J. R., (1994) Oxygen self-diffusion in calcite: Dependence on temperature and water fugacity, *Earth and Planetary Science Letters*, **121**, 575-587
- Fyktilas, M., Innocenzi, F., Manetti, P., Mazzuoli, R., Peccerillo, A., Villari, L., (1984) Tertiary to Quaternary evolution of volcanism in the Aegean region, *In: Robertson, A. H. F., Dixon, J. E., (eds) The geological evolution of the Eastern Mediterranean*. Geological Society, London, Special Publications, **17**, 687-699
- Garrels, R. M., McKenzie, F. T., (1971) Evolution of sedimentary rocks. W. W. Norton & Company, New York, 397 pp
- Hoefs, J., (2009) Stable isotope geochemistry, 6th edition, Springer
- Hofmann, A. W., (1972) Chromatographic theory of infiltration metasomatism and its application to feldspars, *American Journal of Science*, **272**, 69-90
- Jansen, J. B. H., Van der Rijst, H., Rye, R. O., Andriessen, P. A. M., Rye, D. M., (1989) High integrated fluid/rock ratios during metamorphism at Naxos: evidence from carbon isotopes of calcite in schists and fluid inclusions; A discussion of the paper by Kreulen (1988) (Contributions to Mineralogy and petrology, 98, 28-32), *Contributions to Mineralogy and Petrology*, **103**, 123-126
- Jansen, J. B., Schuiling, R. D., (1976) Metamorphism on Naxos: Petrology and geochemical gradients, *American Journal of Science*, **276**, 1225-1253
- Kreulen, R., (1980) CO₂-rich fluids during regional metamorphism on Naxos (Greece): Carbon isotopes and fluid inclusions, *American Journal of Science*, **280**, 745-771
- Kreulen, R., (1988) High integrated fluid/rock ratios during metamorphism on Naxos: Evidence from carbon isotopes of calcite in schists and fluid inclusions, *Contributions to Mineralogy and Petrology*, **98**, 28-32
- Kreulen, R., Van Beek, P. C. J. M., (1983) The calcite-graphite isotope thermometer, data on graphite bearing marbles from Naxos, Greece, *Geochimica et Cosmochimica Acta*, **47**, 1527-1530

- Lassey, K. R., (1982) On computation of certain integrals containing the modified Bessel function $I_0(\zeta)$, *Mathematics of Computation*, **39**, 625-637
- Lassey, K. R., Blattner, P., (1988) Kinetically controlled oxygen isotope exchange between fluid and rock in one-dimensional advective flow, *Geochimica et Cosmochimica Acta*, **52**, 2169-2175
- Lewis, S., Holness, M., Graham, C., (1998) An ion microprobe study of marble from Naxos, Greece: grain-scale fluid pathways and isotopic equilibrium during metamorphism, *Geology*, **26**, 935-938
- Lister, G. S., Banga, G., Feenstra, A., (1984) Metamorphic core complexes of the Cordilleran type in the Cyclades, Aegean Sea, Greece, *Geology*, **12**, 221-225
- O'Neil, J. R., Clayton, R. N., Mayeda, T. K., (1969) Oxygen isotope fractionation in divalent metal carbonates, *Journal of Chemical Physics*, **51**, 5547-5558
- Rye, R. O., Shuiling, R. D., Rye, D. M., Jansen, J. B. H., (1976) Carbon, hydrogen and oxygen isotope studies of the regional metamorphic complex at Naxos, Greece, *Geochimica et Cosmochimica Acta*, **40**, 1031-1049
- Seward, D., Vanderhaeghe, O., Siebenaller, L., Thomson, S., Hibsich, C., Zingg, A., Holzner, P., Ring, U., Duchêne, S., (2009) Cenozoic tectonic evolution of Naxos Island through a multi-faceted approach of fission-track analysis, *Geological Society, London, Special Publications 2009*, **231**, 179-196
- Shuiling, R. D., Kreulen, R., (1979) Are thermal domes heated by CO₂-rich fluids from the mantle? *Earth and Planetary Science Letters*, **43**, 298-302
- Skelton, A. D. L., Graham, C. M., Bickle, M. J., (1995) Lithological and structural controls on regional 3-D fluid flow patterns during greenschist facies metamorphism of the Dalradian of the SW Scottish highlands, *Journal of Petrology*, **36**, 563-586
- Skelton, A. D. L., Valley, J. W., Graham, C. M., Bickle, M. J., Fallick, A. E., (2000) The correlation of reaction and isotope fronts and the mechanism of metamorphic fluid flow, *Contributions to Mineralogy and Petrology*, **138**, 364-375

- Skelton, A. D. L., Whitmars, R., Arghe, F., Cril, P., Koyi, H., (2005) Constraining the rate and extent of mantle serpentinization from seismic and petrological data: implications for chemosynthesis and tectonic processes, *Geofluids*, **5**, 153-164
- Skelton, A. D. L., (2011) Flux rates for water and carbon during greenschist facies metamorphism, *Geology*, online publication with doi:10.1130/G31328.1
- Yardley, B. W. D., (2005) Metal concentrations in crustal fluids and their relationship to ore formation, *Economic Geology*, **100**, 613- 632
- Walther, J. V., Orville, P. M., (1982) Volatile production and transport in regional metamorphism, *Contributions to Mineralogy and Petrology*, **79**, 252-257
- Wark, D. A., Watson, E. B., (2003) Interdiffusion of H₂O and CO₂ in metamorphic fluids at 490° and 690° C and 1 GPa, *Geochimica et Cosmochimica Acta*, **68**, 2693-2698
- Wijbrans, J. R., McDougall, I., (1988) Metamorphic evolution of the Attic Cycladic Massif Belt on Naxos (Cyclades, Greece) utilizing ⁴⁰Ar/³⁹Ar age spectrum measurements, *Journal of Metamorphic Geology*, **6**, 1-23

Appendix A – derivation of transport equations



We can view the fluid-rock system as consisting of the smallest possible, equally shaped and sized cells, or unit volumes. Each such unit volume consists of a fluid-filled pore with the volume V_f , and the surrounding rock of volume V_s . The rock and fluid each hold a mass M_i of the isotopic tracer, denoted $M_{i,s}$ and $M_{i,f}$ respectively.

The equations used for describing the flow of a fluid through a porous medium are derived from the one-dimensional continuity equation, used to describe the conservation of mass

$$\frac{\partial}{\partial t} u + \frac{\partial j}{\partial z} = 0 \quad (1)$$

where u is the total mass of the isotopic tracer per unit volume, and j the flux of u . Equation (1) simply states that the rate of change in mass inside the unit volume must equal the difference in mass flow into and out of it. u is defined as

$$u = \frac{M_{tot}}{V_{tot}} \quad (2)$$

where

$$M_{tot} = M_{i,f} + M_{i,s} \quad (3)$$

and

$$V_{tot} = V_f + V_s \quad (4)$$

We want to express u as a function of the isotopic concentration instead of mass, since this is what we obtain from the analyses. The mass of the isotopes is the product of the volume, density and concentration. Equation (2) is rewritten to the form

$$u = \frac{1}{V_{tot}} (V_f \rho_f C_f + V_s \rho_s C_s) \quad (5)$$

where ρ is the density of the fluid (f) or solid (s) and C the concentration of the isotope in the fluid (f) and solid (s) phase respectively.

The porosity, φ , within the system is defined as the fraction of the unit volume which is fluid-filled

$$\varphi = \frac{V_f}{V_{tot}} \quad (6)$$

In the pinned boundary model, the assumption is made that the system is in grain-scale equilibrium, meaning the rate of exchange between the fluid and the solid is relatively fast compared to the rate of fluid flow. The equilibrium condition is set to

$$K_d = \frac{C_s}{C_f} \quad (7)$$

where K_d is the partition coefficient by mass of the isotope between the fluid and the rock.

By combining equations (5) to (7) we get the final expression for u (i.e. mass of isotope per unit volume) for the pinned boundary model:

$$u = C_f \rho_f \left(\varphi + \frac{\rho_s K_d}{\rho_f} (1 - \varphi) \right) \quad (8)$$

The second term of equation (1) expresses the change in the flux of u along the z-direction. In the pinned boundary model both advection and diffusion contributes to the flux of the isotopic tracer in the direction of fluid flow and j can therefore be defined as:

$$j = j_{adv} + j_{diff} \quad (9)$$

where j_{adv} is the flux contributed by advection and j_{diff} is the flux contributed by diffusion. The flux contributed by advection is only dependent on the fluid flow velocity, ω :

$$j_{adv} = \omega u \quad (10)$$

where u describes the mass of the isotopic tracer in the *mobile* fluid phase per unit volume, meaning:

$$j_{adv} = \omega \frac{M_{i,f}}{V_{tot}} \quad (11)$$

remembering the definition of the porosity (equation 6) and that the mass of the isotopic tracer in the fluid phase is the product of the volume of fluid, density of the fluid and concentration of tracer within the fluid phase, equation (11) is rewritten to

$$j_{adv} = \omega \varphi \rho_f C_f \quad (12)$$

The diffusion of the isotopic tracer through the solid crystal network is neglected, and only considered within the fluid phase in the z -direction, and is expressed as:

$$j_{diff} = -D \frac{\partial u}{\partial z} \quad (13)$$

where D is the diffusivity coefficient of the isotope in the fluid phase, z the direction of fluid flow and u the mass of isotope in the fluid phase per unit volume. The expression is rewritten to the form:

$$j_{diff} = -D \frac{\partial}{\partial z} \left(\frac{M_{i,f}}{V_{tot}} \right) = -\varphi D \rho_f \frac{\partial C_f}{\partial z} \quad (14)$$

By inserting the final expression of equation (14), (12) and (8) into equation (1) we get the final expression for the pinned boundary model as:

$$\left(\varphi + \frac{\rho_s K_d}{\rho_f} (1 - \varphi) \right) \frac{\partial C_f}{\partial t} + \omega \varphi \frac{\partial C_f}{\partial z} = \varphi D \frac{\partial^2 C_f}{\partial z^2} \quad (15)$$

For the linear kinetic exchange model, u in equation (1) is derived in the same manner as for the pinned boundary model above, only rewritten to the form:

$$u = (1 - \varphi)\rho_s \left(C_s + \frac{V_f \rho_f}{V_s \rho_s} C_f \right) \quad (16)$$

which aids with simplifications of the equations made at a later stage.

In the linear kinetics exchange model, the flow velocity of the fluid within the equally paced cracks or conduits is considered to be fast compared to the rate of exchange between the fluid and the solid, and the condition of equilibrium used for the pinned boundary model is not applicable in this case. This relatively fast fluid flow also has the effect that diffusion in the z-direction can be ignored, since it is a much slower process than the advection within the fluid conduits. The exclusion of diffusion gives an expression for j as:

$$j = \omega \frac{V_f \rho_f C_f}{V_{tot}} \quad (17)$$

where the numerator equals the mass of the isotope within the fluid phase. Equation (16) and (17) is inserted into equation (1) giving:

$$(1 - \varphi)\rho_s \frac{\partial}{\partial t} \left(C_s + \frac{V_f \rho_f}{V_s \rho_s} C_f \right) + \frac{V_f \rho_f}{V_{tot}} \omega \frac{\partial C_f}{\partial z} = 0 \quad (18)$$

Using the definition of the porosity from equation (6) and the expression:

$$\frac{\varphi \rho_f}{\rho_s (1 - \varphi)} = \Phi' \quad (19)$$

gives the final expression for the linear kinetic mass balance equation as:

$$\frac{\partial}{\partial t} (\Phi' C_f + C_s) + \Phi' \omega \frac{\partial C_f}{\partial z} = 0 \quad (20)$$

Appendix B –Results from XRF analysis

Major elements

Z	Mg	Al	Si	S	Cl	K	Ca	Fe	Ni	Zr	Ag	Cd	Sn	Sb	LE	SUM
(m)	%	%	%	%	%	%	%	%	%	%	%	%	%	%	%	
-0.94		0.88	2.07	0.03		0.08	42.23	0.18		0.003	0.02	0.03	0.03	0.04	54.40	99.99
-0.47		5.36	15.93			1.53	14.31	3.60		0.010	0.02	0.02	0.03	0.03	58.66	99.50
-0.09		5.44	14.42			1.45	11.76	3.96		0.010	0.02	0.03	0.03	0.04	62.29	99.44
-0.19		2.82	11.74			0.96	15.98	3.17		0.008	0.02	0.02	0.02	0.04	64.73	99.51
0.02	2.35	1.88	4.46	0.26	1.67	0.08	36.64	1.02	0.01	0.007	0.02	0.03	0.03	0.03	51.47	99.95
0.04	5.52	3.50	7.91	0.10			31.03	0.68	0.01	0.005	0.02	0.03	0.03	0.03	51.06	99.94
0.06		0.29	0.42	0.03	2.12	0.05	44.77	0.04		0.008	0.02	0.03	0.04	0.04	52.16	100.00
0.08			0.34			0.13	42.07	0.04		0.010	0.02	0.03	0.03	0.04	57.29	100.00
0.09		0.16	0.43	0.02	8.65	0.11	41.79	0.06		0.005		0.03		0.03	48.70	100.00
0.11		0.11	0.26		6.33		42.58	0.04		0.003	0.02	0.03	0.03	0.03	50.57	100.00
0.13		1.37	3.14	0.54	2.18	0.15	38.54	0.31		0.007	0.02	0.03	0.03	0.04	53.63	99.98
0.15			0.38		1.77	0.12	41.85	0.06		0.005		0.03			55.77	99.99
0.17		0.13	0.32	0.03	1.83	0.12	39.89	0.02		0.005	0.03	0.03		0.04	57.47	99.91
0.19			0.40		1.86	0.12	39.01	0.04		0.005			0.03		58.53	100.00
0.23			0.53			0.15	38.14	0.07		0.006		0.04		0.05	61.01	99.99
0.28			0.48				38.25	0.08							61.18	99.99
0.33		0.30	0.87	0.04		0.16	40.46	0.09			0.02	0.03	0.03	0.03	57.95	99.99
0.38		0.24	0.55			0.05	41.79	0.08		0.003	0.02	0.02	0.04	0.04	57.16	100.00
0.47		0.73	1.43	0.04	1.85	0.16	39.91	0.25	0.01	0.004	0.02	0.03	0.03	0.04	55.35	99.86
0.56		0.45	0.94			0.17	38.12	0.32		0.004	0.03	0.03	0.03	0.03	59.77	99.90
0.66		0.54	1.37			0.12	42.02	0.21			0.02	0.03	0.03	0.04	55.52	99.89
0.75		0.64	1.63	0.21	3.05	0.14	40.00	0.25			0.02	0.03	0.03	0.03	59.26	105.29
0.85		0.20	1.13	0.38	2.92	0.28	35.52	0.23				0.04		0.04	53.96	94.69
0.94		0.21	0.60		1.48		40.88	0.12		0.004	0.02	0.03	0.03	0.03	56.59	99.99
1.13		1.01	2.32	0.06		0.33	36.47	0.58		0.005	0.02	0.03		0.04	59.09	99.97
1.32		0.70	1.38	0.03		0.21	38.90	0.20		0.004		0.03		0.03	58.51	100.00
1.50		0.15	0.62			0.15	38.43	0.08			0.02	0.03	0.03	0.04	60.45	100.00
1.69			0.42		2.83	0.09	43.20	0.07			0.02	0.03	0.03		53.30	100.00
1.88		0.19	0.41		2.37	0.15	40.27	0.07			0.02	0.02		0.03	56.45	99.99
2.07		0.50	1.13			0.15	40.71	0.11			0.03	0.03	0.03	0.04	57.17	99.90
2.26		0.46	0.94			0.08	40.64	0.15		0.004	0.02	0.03	0.03	0.03	57.60	99.99
2.44		0.37	1.07		5.40	0.19	39.87	0.40			0.02	0.03		0.03	52.60	99.99
2.63		0.99	1.91	0.02		0.25	39.14	0.69				0.02	0.02	0.03	56.79	99.86
2.82		0.32	1.11			0.30	39.15	0.49						0.04	58.57	99.98
3.29	0.89	0.45	0.89	0.03		0.03	41.32	0.06	0.01	0.003	0.03	0.03	0.03	0.04	56.13	99.94
3.76		0.37	1.22	0.24	2.75	0.03	42.66	0.07		0.005	0.02	0.03	0.03	0.03	52.48	99.93
4.23		0.82	2.01	0.37	4.66	0.14	38.38	0.22		0.003	0.02	0.03	0.03	0.03	53.27	99.99
4.70		0.53	1.24	0.31		0.04	40.42	0.11			0.02	0.03	0.03	0.04	57.16	99.92
5.17			0.17			0.05	41.33	0.02			0.02	0.03	0.03	0.04	58.33	100.00
5.64		0.23	0.54		2.04		37.74	3.42			0.02	0.03	0.03	0.03	55.67	99.74

Z	Mg	Al	Si	S	Cl	K	Ca	Fe	Ni	Zr	Ag	Cd	Sn	Sb	LE	SUM
(m)	%	%	%	%	%	%	%	%	%	%	%	%	%	%	%	%
6.39		0.43	1.07			0.05	38.74	0.17			0.03	0.03	0.03	0.04	59.37	99.96
6.86		0.21	0.38	0.03			41.24	0.04			0.02	0.03	0.03	0.04	57.98	100.00
7.52		0.47	1.33	0.18		0.11	38.53	0.10			0.02	0.03			59.14	99.91
7.99		0.11	0.44	0.03	1.60	0.05	38.80	0.04			0.02	0.03	0.03	0.03	58.82	99.99
8.46			0.30		2.86	0.08	35.68	0.05				0.03	0.04		60.97	100.00
8.93		0.44	1.35	0.33	1.94	0.10	40.73	0.09			0.02	0.03	0.03	0.04	54.92	100.00
9.40			0.37			0.06	36.92	0.04			0.02	0.03	0.03	0.04	62.50	100.00
9.87		0.20	0.48		1.79	0.11	37.77	0.06		0.004	0.03	0.02		0.03	59.43	99.93
10.34		0.19	0.46	0.05	1.29	0.03	41.70	0.03	0.01		0.02	0.03	0.03	0.04	56.12	99.99
10.81			0.27		1.52	0.10	41.09	0.03			0.02	0.03	0.03	0.04	56.87	100.00
11.28	1.99		0.52		2.30	0.15	40.40	0.06				0.03			54.54	99.99
11.75		0.87	2.37	0.39	1.58	0.10	39.99	0.20			0.02	0.02	0.02	0.04	54.38	99.99
12.22			0.34		2.00	0.10	39.00	0.03				0.03		0.04	58.38	99.92
12.69		0.15	0.50	0.03	1.46	0.04	40.88	0.04			0.02	0.03	0.03	0.03	56.79	100.00
13.16		0.36	0.70	0.02		0.03	41.12	0.04		0.003	0.02	0.03	0.03	0.04	57.61	100.00
13.63		0.26	0.67	0.02			41.74	0.03			0.02	0.03	0.03	0.03	57.15	99.99
14.10		0.80	1.83	0.05		0.10	39.87	0.12			0.02	0.03	0.03	0.03	57.11	99.99
14.57		0.37	0.60		1.38	0.08	39.59	0.04				0.02	0.03	0.04	57.85	100.00
14.57			0.32		4.09	0.04	38.87	0.04				0.02		0.04	56.57	100.00
14.66		0.43	1.15	0.36	1.62	0.06	42.31	0.08			0.02	0.03	0.03	0.04	53.86	99.99
14.75		0.26	1.04	0.25	3.65	0.07	41.91	0.06			0.02	0.03	0.03	0.04	52.64	100.00
14.85		0.52	1.62	0.30	2.26	0.12	40.49	0.17			0.02	0.03		0.04	54.42	99.99
14.94		0.63	2.20	0.32	1.15	0.23	38.01	0.22			0.02	0.03	0.03	0.04	57.08	99.98
15.04		0.44	1.58	0.34	0.93	0.09	40.02	0.11			0.02	0.03	0.03	0.05	56.35	99.99
15.13			0.29			0.08	40.44	0.03			0.02	0.03	0.03	0.04	59.04	100.00
15.22		0.19	0.29		3.84	0.05	39.16	0.04			0.02	0.03	0.03	0.03	56.33	100.00
15.32		0.84	2.49	0.45		0.11	38.91	0.18		0.005	0.02	0.03	0.03	0.03	56.80	99.91
15.41	1.13	0.70	2.40	0.34		0.15	39.10	0.23		0.003	0.02	0.04	0.04	0.04	55.81	99.99
15.50		0.63	1.95	0.35	2.79	0.09	41.23	0.11			0.02	0.03	0.03	0.04	52.72	99.99
15.60		0.91	2.96	0.37		0.20	37.26	0.25			0.02	0.03		0.03	57.88	99.90
15.65		0.56	1.71	0.30	2.40	0.18	37.70	0.12						0.04	56.98	99.99
15.69		0.58	1.56	0.30	2.18	0.13	38.69	0.14			0.02	0.03	0.03	0.03	56.30	99.99
15.74		1.08	2.57	0.39		0.09	39.32	0.18			0.02	0.03	0.03	0.04	56.17	99.92
15.79		0.29	1.10	0.25	2.39	0.15	41.50	0.07			0.02	0.04	0.03	0.04	54.12	100.00
15.83		1.01	3.08	1.39	2.23	0.16	37.75	0.26			0.02	0.03	0.03	0.04	53.91	99.91
15.88		0.99	2.87	0.40	2.84	0.17	39.97	0.25			0.02	0.03	0.03	0.04	52.37	99.99
15.93		1.31	3.31	0.16		0.24	38.86	0.55		0.004	0.02	0.03	0.02	0.03	55.34	99.88
15.97		0.51	1.12	0.12		0.15	40.23	0.37			0.02	0.03	0.03	0.05	57.35	99.98
16.02		0.68	1.94	0.22		0.31	33.93	0.94		0.005		0.04	0.03	0.04	61.81	99.95
16.07	2.41	0.59	2.25	0.38	2.88	0.04	35.30	0.10			0.02	0.03	0.03	0.04	55.91	99.98
16.12		1.22	3.83	0.44	1.67	0.18	37.34	0.21		0.004	0.02	0.04	0.03	0.04	54.89	99.91
16.16		0.13	0.35		2.16	0.04	41.49	0.04			0.02	0.03	0.03	0.04	55.68	100.00
16.21		0.66	1.70	0.29	2.91	0.09	40.57	0.15		0.003	0.02	0.03	0.03	0.04	53.49	99.99

Z	Mg	Al	Si	S	Cl	K	Ca	Fe	Ni	Zr	Ag	Cd	Sn	Sb	LE	SUM
<i>(m)</i>	%	%	%	%	%	%	%	%	%	%	%	%	%	%	%	
16.26		0.25	8.31	0.09			36.92	0.09		0.004	0.03	0.04	0.03	0.04	54.11	99.91
16.30		0.22	0.95	0.08	2.03	0.06	39.67	0.05		0.005	0.02	0.02	0.03	0.03	56.84	100.00
16.35		0.49	4.55	0.50	1.05	0.08	39.19	0.11			0.02	0.03	0.03	0.04	53.90	99.99
16.38		0.48	1.66	0.41	4.61	0.09	39.42	0.13	0.01		0.02	0.03	0.03	0.04	53.08	100.00
16.41		0.62	2.15	0.80	1.80	0.15	37.91	0.17			0.02	0.03		0.04	56.19	99.89
16.43		0.56	1.53	0.30	3.80	0.20	35.61	0.22			0.02	0.03	0.03	0.04	57.63	99.99
16.44	0.88	0.87	2.49	0.48		0.12	33.42	0.20			0.02	0.02	0.03	0.04	61.34	99.90
16.46	2.08	0.53	2.25	0.34		0.09	35.86	0.10			0.02	0.03	0.03	0.04	58.63	99.99
16.48		0.45	1.30	0.27	2.53	0.07	39.77	0.14			0.02	0.03	0.03	0.04	55.33	99.99
16.50		0.37	1.68	0.26	3.05	0.12	34.83	0.17			0.02	0.03			59.48	100.00
16.52		0.54	1.90	0.31	2.05	0.13	38.92	0.20		0.004	0.02	0.03	0.04	0.04	55.79	99.98
16.56		3.73	13.76	1.06		2.81	21.26	2.29		0.013	0.02	0.03	0.04	0.03	54.52	99.57
16.59		2.87	10.57	7.79		0.62	12.47	2.51		0.009	0.02	0.03	0.03	0.04	62.72	99.68
16.63	1.12	3.65	11.42	0.19		1.35	19.86	3.62	0.02	0.014	0.03	0.03	0.03	0.05	57.95	99.32
16.69		0.42	3.35	0.20		0.08	38.55	0.14			0.02	0.03	0.03	0.04	57.07	99.93
16.71	0.81	0.18	0.69	0.05	2.22	0.08	42.33	0.16	0.01		0.02	0.03	0.03	0.04	53.33	99.99
16.73		0.30	0.85	0.04	2.26	0.06	41.57	0.10			0.02	0.03	0.02	0.04	54.63	99.93
16.75		0.56	1.28	0.11		0.14	41.82	0.17			0.03	0.03	0.04	0.04	55.77	99.99
16.76	1.13	0.46	1.39	0.03	0.99	0.19	38.86	0.18			0.03	0.03	0.03	0.04	56.63	99.99
16.79		0.43	1.46	0.17		0.24	36.15	0.52			0.02	0.03	0.03	0.04	60.81	99.89
16.82		0.45	1.30	0.16		0.10	37.38	0.15			0.03	0.03	0.03	0.05	60.23	99.90
16.85		0.42	1.40	0.23	4.47	0.08	40.75	0.12		0.004	0.02	0.03	0.03	0.03	52.42	100.00
16.87		0.97	2.85	0.57		0.19	40.43	0.22		0.003	0.02	0.03	0.03	0.04	54.52	99.88
16.89	1.22	1.15	3.63	0.52		0.20	37.81	0.27		0.000	0.02	0.02	0.03	0.04	55.01	99.92
16.91		1.58	3.89	0.64		0.16	40.49	0.31	0.01	0.003	0.02	0.03	0.02	0.04	52.78	99.98
16.92		0.93	3.09	0.29		0.11	40.70	0.18		0.004	0.02	0.03	0.03	0.04	54.49	99.91
16.96		4.20	12.67	0.16		1.53	17.66	3.37	0.01	0.000	0.02	0.03	0.03	0.04	59.50	99.22
17.10	1.59	6.76	17.19			3.13	1.78	7.83		0.012	0.02	0.03	0.03	0.04	60.74	99.15
17.38		3.85	23.14	3.23		1.10	6.36	2.59	0.01	0.017	0.02	0.03	0.03	0.04	59.19	99.59
17.67	0.74	5.27	26.55	1.48		1.19	4.09	3.54	0.02	0.015	0.02	0.03	0.03	0.05	56.44	99.46

Minor elements

Z	Ti	V	Mn	Ni	Cu	Zn	As	Rb	Sr	Y	Pb	Zr
(m)	ppm	ppm	ppm	ppm	ppm	ppm	ppm	ppm	ppm	ppm	ppm	ppm
-0.94	223	14	30			11		5	216	5	10	
-0.47	2564	68	333	26	27	51	4	94	74	21	12	101
-0.09	2121	50	435	72	25	45	7	52	28	12	40	83
-0.19	2630	53	755	31	27	57		97	38	20	20	92
0.02	166	13	68	39		15			405			
0.04	56	60	32	37		69	5		365		6	
0.06	28								463			
0.08	29					8			531			
0.09									438	4		12
0.11	430	17	91	44	17	10		5	158	4		9
0.13	330		99	56	15	12		7	535		8	
0.15	71								317		9	
0.17					18				248			
0.19	63								296			
0.23	306					7			227			
0.28	103	15		30		9			227	4	9	8
0.33	34								200			
0.38	204	11				11		4	131		13	8
0.47	330	14	26			15	5	8	124			18
0.56	161	9	31	45	13	12		8	430	4		14
0.66	738		65		15	12		15	193	4	11	14
0.75	151					9		5	177			9
0.85	252							12	177	4		15
0.94	396	8	40		19	8		8	55	9		14
1.13	99					13		4	128	5	7	
1.32	70							4	190	4		7
1.50	146	9				14		10	173	5		9
1.69	48								165			
1.88	100		44			10		4	147			
2.07	174	9			16	9	5	11	178			8
2.26	155	12				15		17	163	4		9
2.44	110							4	172			8
2.63	624	18	46			18		17	177		6	26
2.82	245				17	16		7	143	5		9
3.29	138								141			
3.76	99					8			217			
4.23	210					7			149			7
4.70	141					8			105			
5.17									102			6
5.64	30			35				3	27	5		

Z	Ti	V	Mn	Ni	Cu	Zn	As	Rb	Sr	Y	Pb	Zr
<i>(m)</i>	<i>ppm</i>	<i>ppm</i>	<i>ppm</i>	<i>ppm</i>	<i>ppm</i>	<i>ppm</i>	<i>ppm</i>	<i>ppm</i>	<i>ppm</i>	<i>ppm</i>	<i>ppm</i>	<i>ppm</i>
6.39	57					7			61			
6.86	61								109			
7.52	179								114			8
7.99	60								171			
8.46	56								122			
8.93	192					6		3	123			
9.40	348			30		10		5	93			6
9.87	88					9			146			
10.34	61					6			139		6	
10.81									104		7	6
11.28	106							4	87	4		
11.75	256								122		6	7
12.22	61								112			
12.69	73								100			
13.16	55					6			100			
13.63	84			33	11				171			
14.10	211					7	4		95			
14.57	80								137			
14.57	46								57			
14.66	66								56			
14.75	115					9			88			
14.85	262				12				134			7
14.94	380	10				9			108			9
15.04	188	8							91			
15.13	366		31	43		10		3	126		6	6
15.22	292	13				7	5	4	155			10
15.32	395								161	4		8
15.41	281					7		5	196			
15.50	177							4	136		7	
15.60	464	9	20		14	8		3	148			
15.65	299					7			83			
15.69	122								92			
15.74	164								83			
15.79	136					8			83			
15.83	344		24		15	8			80			
15.88	155							3	69			
15.93	179	10		36		12		5	117	4	7	14
15.97	238	19	55		15	29		12	110	5	10	9
16.02	269	11	30			12	5	13	151	4		20
16.07	164					8			122		6	5
16.12	267		67		12	10			159			
16.16	35					6			180			
16.21	161								144			

Z	Ti	V	Mn	Ni	Cu	Zn	As	Rb	Sr	Y	Pb	Zr
<i>(m)</i>	<i>ppm</i>	<i>ppm</i>	<i>ppm</i>	<i>ppm</i>	<i>ppm</i>	<i>ppm</i>	<i>ppm</i>	<i>ppm</i>	<i>ppm</i>	<i>ppm</i>	<i>ppm</i>	<i>ppm</i>
16.26	47		28						157			
16.30	153		28						292			
16.35	147					6			131		5	8
16.38	190					6			152			
16.41	264					10	5		158			
16.43	221								151			
16.44	243		41	30		7			157	5		
16.46	178		38						120			
16.48	237	7	62	31		10			132			6
16.50	179		28					3	183	3		
16.52	229		66		13	6			209	4		7
16.56	1438	60	415	75	18	38		60	217	14	6	216
16.59	1739	84	723	111	36	49		83	310	16	14	189
16.63	1232	48	898	70		28		39	437	18	19	96
16.69	452	9	35		13	15	5	3	185			
16.71	494		23			20		4	111			
16.73	384					8			142		11	
16.75	375					11		5	148			
16.76	420		27	31		11		5	167			
16.79	278	10	32			16		11	107			9
16.82	172			30					124			
16.85	174		20			7		4	162			
16.87	367		24			8		4	164			10
16.89	446	9	34			8			135	3		9
16.91	394	7	26			7		4	116			6
16.92	209				13	13			219	3		
16.96	3378	88	1301	81	25	80		53	154	20	26	107
17.10	4457	100	762		19	110		131	171	11	21	79
17.38	2330	46	401	70	17	31		56	202	15	13	184
17.67	2946	103	1886	139	32	48	7	52	191	20	9	144